White Paper

# IQ•SPECT:

## a technical and clinical overview

**Partha Ghosh, MD**
Siemens Healthineers
Molecular Imaging Business Line

siemens.com/iqspect

SIEMENS Healthineers

# Introduction

One of the key trends in nuclear medicine is the ever-increasing demand for faster myocardial perfusion imaging (MPI). IQ•SPECT is a fast cardiac imaging solution that is offered on our Symbia™ SPECT and SPECT/CT systems. It uses a combination of converging collimators, modified cardio-centric acquisition, and special reconstruction methods to deliver ultrafast cardiac imaging 4 times faster than conventional SPECT acquisition, with scan times as low as 4 minutes per acquisition. This unique approach can be combined with or added to a general-purpose gamma camera or SPECT/CT so the system is able to perform all routine clinical applications, as well as ultrafast cardiac scans, with just a change in collimator and acquisition mode. This approach improves the flexibility and versatility of the general-purpose gamma camera or SPECT/CT, enabling departments to perform a larger volume and a wider range of procedures without additional dedicated equipment and space requirements. This white paper briefly explains the technical aspects of IQ•SPECT and demonstrates normal patterns and variations, as well as shows a series of clinical examples of ischemia and infarction to familiarize nuclear cardiologists with IQ•SPECT.

## IQ•SPECT: technical considerations

In nuclear medicine studies, image quality is limited by the number of detected photons. When imaging a small organ, such as the heart, much of the large-field-of-view detector on a conventional gamma camera is not used. One way to increase the number of detected photons is to utilize more of the detector by using a fan-beam or cone-beam collimator to magnify the projection of the organ on the detector. The cost of this increase in detected photons is a reduction in the transverse or axial field of view, or both, leading to truncation artifacts in reconstructed images. IQ•SPECT is an advanced MPI solution that avoids the problem of truncated data by employing a variable focus collimator, retaining the magnifying properties of a cone-beam collimator near the center of the field of view, and eliminating truncation at the edges of the field of view, similar to a parallel-hole collimator.

IQ•SPECT is an intelligent solution, collecting 4 times as many counts from the heart during a myocardial perfusion SPECT study on a Symbia imaging system while maintaining the same resolution as a low-energy, high-resolution collimator. The additional counts can be used to reduce the acquisition time or reduce the injected dose by up to 75 percent. This flexibility also allows optimized combination of a reduction in injected dose together with a decrease in acquisition time to suit individual department requirements. IQ•SPECT consists of three components: **SMART**ZOOM collimators, a cardio-centric acquisition, and the IQ•SPECT reconstruction. **SMART**ZOOM collimators are designed so that the center of the field of view magnifies the heart, while the edges sample the entire body to avoid the truncation artifacts common to pinhole and focusing collimators. It is important to note that the **SMART**ZOOM collimator achieves a gain in counts without compromising image resolution, as is the case with conventional, large bore, parallel-hole collimators. IQ•SPECT takes advantage of the flexible gantry motions available on the Symbia platform to perform a cardio-centric acquisition. The cardio-centric orbit allows the detectors to rotate around a virtual center of rotation that is positioned so the heart is always in the most sensitive area of the collimator, also known as the "sweet spot." The IQ•SPECT reconstruction algorithm models the unique position and shape of each of the 48,000 **SMART**ZOOM collimator holes and fully characterizes the location and orientation of the detectors as the gantry rotates. IQ•SPECT reconstruction also includes resolution recovery, CT-based attenuation correction, and energy window-based scatter correction.

**SMARTZOOM collimation**

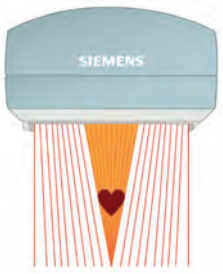


**Cardio-centric acquisition**

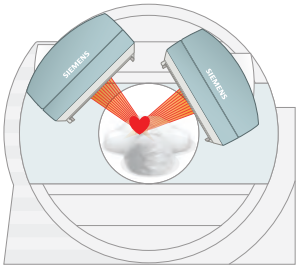


**IQ•SPECT reconstruction**


## SMARTZOOM collimation

Cast collimation manufacturing techniques have been used to fabricate the unique geometry of the **SMART**ZOOM collimators. The focus of each collimator varies continuously from cone-like in the central region to parallel at the edges. This provides magnification of the cardiac region while avoiding truncation of the surrounding tissue. The unique position and shape of each hole in the collimator, also referred to as a vector map, is measured in our factory and stored with the collimator to be used during reconstruction.

## Cardio-centric acquisition

For optimal sensitivity gain, the heart should remain in the **SMART**ZOOM "sweet spot" in all views. IQ•SPECT uses the flexibility of the Symbia gantry to achieve this focus throughout the acquisitions. During patient setup, the location of the heart can be easily identified on the patient positioning monitor. IQ•SPECT then computes and executes an orbit that optimizes the gain and image quality for the specific patient.

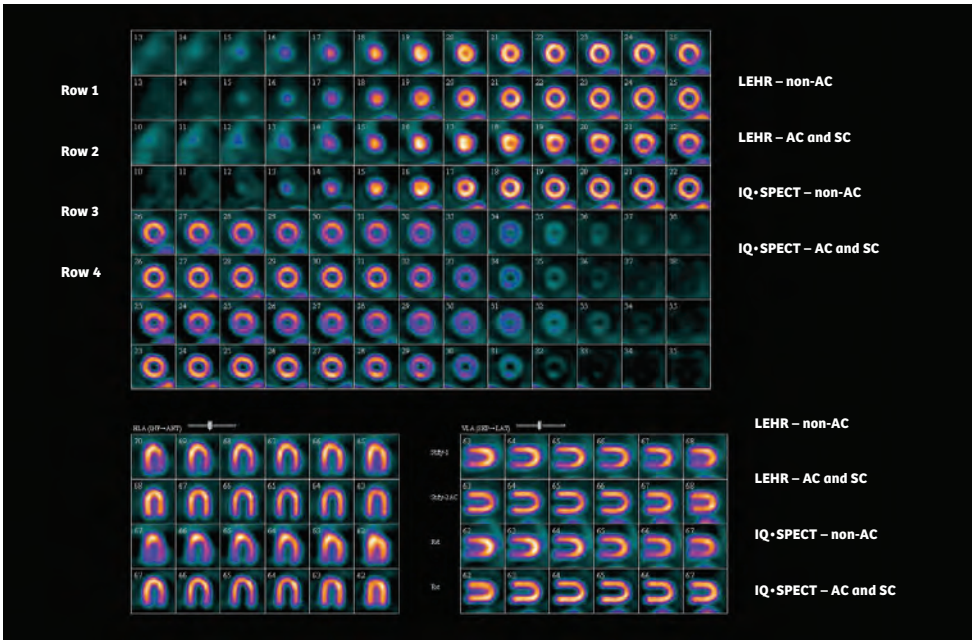


**Figure 1:** Torso phantom study (Data Spectrum).

Unlike a conventional acquisition (or orbit) where the detectors maintain close proximity to the patient, the detectors in the cardio-centric orbit are at a fixed 28 cm from the center of the heart to maintain its position in the collimator "sweet spot." The larger collimator distance also increases patient comfort and may reduce motion artifacts. The unique cardio-centric configuration exploits the flexibility of the Symbia gantry to position each detector at the optimal distance from the user-identified heart over the expected variation of patient population. The angular separation of the detectors is slightly less than the traditional 90 degrees, which improves angular sampling over the most information-rich portion of the cardiac orbit. The cardio-centric acquisition has a scan arc of 208 degrees (104 degrees per head) to compensate for the fan angle of the **SMART**ZOOM collimator and to ensure complete sampling. The angle between the detectors is set to 76 degrees.

## Acquisition

Both gated and non-gated acquisitions of $^{99m}$Tc or $^{201}$Tl are supported. The entire patient setup adds just one additional step to identify the position of the heart on the touch screen patient positioning monitor. The patient is placed on the bed in either a supine or prone position and moved under the nuclear detectors until the heart is approximately centered in the axial direction. The center of the projection of the heart on each detector is marked on the patient positioning monitor, allowing for the calculation of the location of the patient's heart in 3-dimensional space. This will become the center of the cardio-centric orbit. The acquisition can then be started.

## Reconstruction

After data acquisition is complete, the study is transferred to the reconstruction workstation. The projection data should be reviewed for motion and motion correction applied, if necessary. Gated reconstructions with 8 time bins are completed within 90 seconds, and non-gated reconstructions are completed in less than 60 seconds.

The IQ•SPECT reconstruction method is a proprietary implementation of a conjugate-gradient iterative reconstruction algorithm. It has been developed to achieve the following objectives:

- Maintain the same reconstructed resolution as LEHR collimators in a non-circular orbit
- Realize the four-fold sensitivity gain of the **SMART**ZOOM collimator
- Correct for the effects of patient attenuation, scatter, and motion
- Perform reconstructions in a clinically acceptable time

The quality of the reconstructed images can be appreciated by reviewing the results of the following phantom study in Figure 1. A Data Spectrum normal male anthropomorphic torso phantom was loaded with 74, 370, and 407 MBq of $^{99m}$Tc in the heart, liver, and background, respectively, corresponding to typical clinical concentrations of $^{99m}$Tc Sestamibi found in humans.

Careful examination of the non-attenuation and scatter-corrected data in rows 1 and 3 in Figure 1 show some differences between the LEHR and IQ•SPECT reconstructed data.

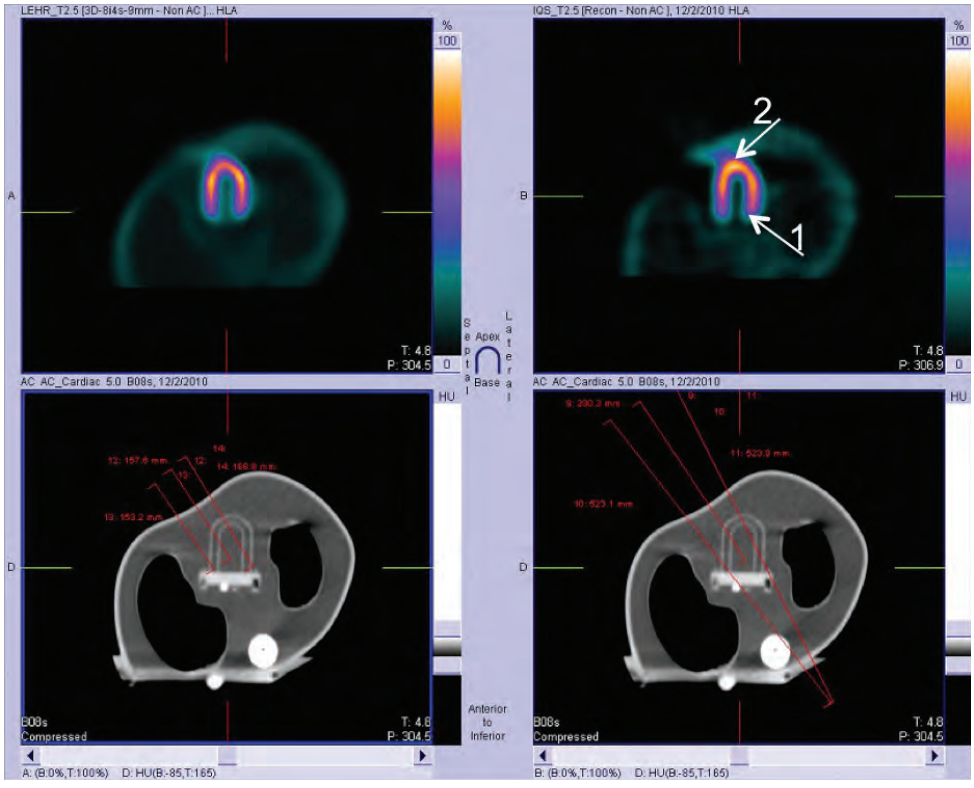


**Figure 2:** Data Spectrum phantom showing effects of attenuation.

The physical characteristics of the collimator and the data acquisition process that lead to these differences can be readily understood by reviewing the images in Figure 2. LEHR images are on the left and IQ•SPECT images are on the right. The bottom two images show a CT scan of the Data Spectrum phantom. Red lines that indicate the lines of sight of the collimator holes are overlaid on the CT images. The images on the top are the resulting reconstructed images. Longer attenuation paths from the most interior part of the heart to the surface of the phantom lead to more deep tissue attenuation (Arrow 1). More counts from tissue closest to the surface lead to an increase in reconstructed counts near the apex (Arrow 2). While there are differences between LEHR and IQ•SPECT reconstructed data when not corrected for attenuation and scatter, the differences are consistent and reproducible. There are new patterns to be learned.

## Workflow

IQ•SPECT is seamlessly integrated with Symbia imaging systems. The **SMART**ZOOM collimator can be included in the Integrated or Automatic Collimator Changers. Automatic Quality Control will perform all common system calibrations for the **SMART**ZOOM collimators. Extreme care has been given to ensure simple and intuitive user interaction.

## IQ•SPECT: technical considerations

### Normal patterns

Comparisons of standard myocardial perfusion SPECT studies using low-energy, high-resolution (LEHR) collimators with filtered back projection (FBP) and 3D Iterative (Flash 3D) reconstruction to IQ•SPECT studies, performed at the same sitting, demonstrate the comparable nature of the two acquisition approaches in terms of tracer distribution patterns, as well as cardiac shape and size. However, there are differences between conventional SPECT and IQ•SPECT reconstructed slices in relation to the shape of the heart, myocardial thickness, effect of attenuation, etc., which require familiarization with the normal patterns of IQ•SPECT myocardial perfusion imaging for effective interpretation. The following clinical examples illustrate such normal patterns.

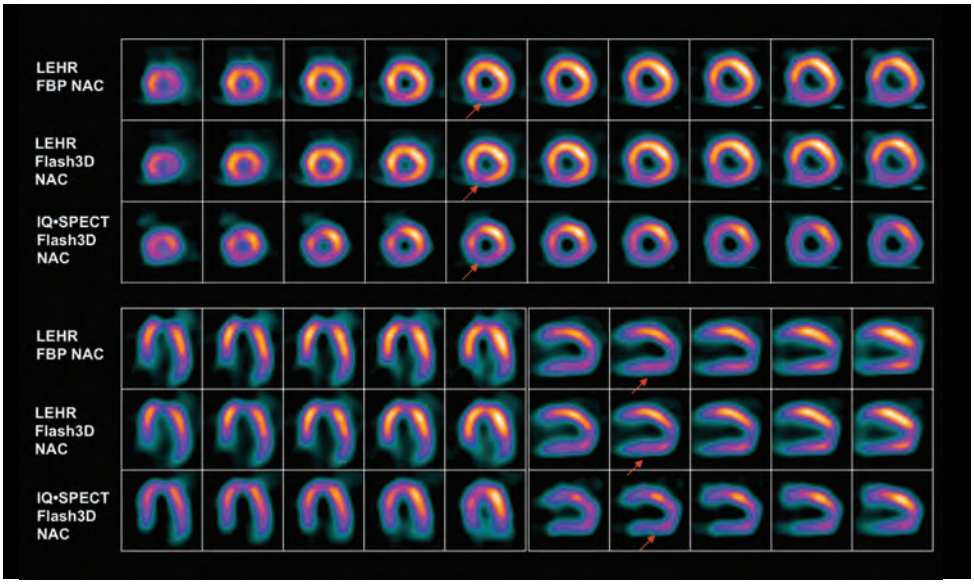


**Figure 3a:** Data courtesy of the University of Michigan, Ann Arbor, MI, USA.

**Figure 3a:** A normal male patient underwent myocardial perfusion imaging with $^{99m}$Tc-MIBI using LEHR and IQ•SPECT. The IQ•SPECT acquisition was four times faster than LEHR acquisition based on standard acquisition protocols. FBP and Flash 3D reconstruction from LEHR acquisition (top and middle rows) are compared to IQ•SPECT reconstruction, also performed using Flash 3D (bottom row). A comparison of the images shows the sharper ventricular margins, as well as slightly smaller left ventricle (LV) size with IQ•SPECT. Note the increased attenuation effect in the inferior and posterobasal wall (red arrows) with IQ•SPECT, compared to the FBP and Flash 3D reconstructions.

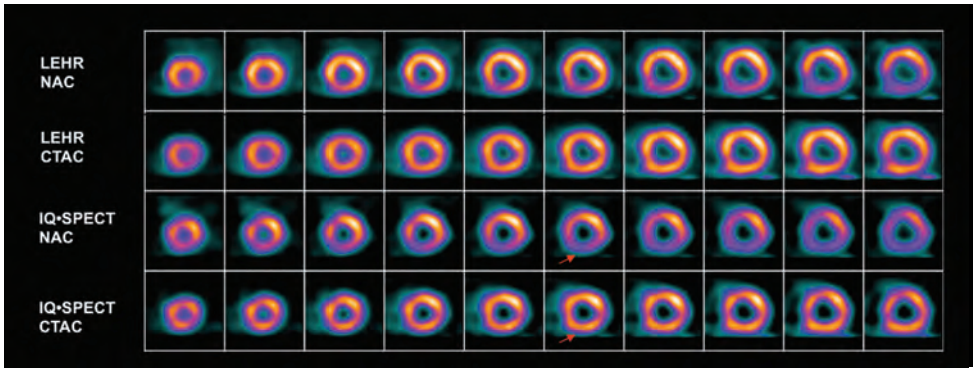


**Figure 3b:** Data courtesy of the University of Michigan, Ann Arbor, MI, USA.

**Figure 3b:** The same patient data is displayed with stress LEHR and IQ•SPECT short axis images with and without computed tomography attenuation correction (CTAC). Note the improvement in uptake in the inferior wall following CTAC in the LEHR study, which is a typical demonstration of attenuation correction. However, the extent of inferior wall attenuation at the same slice level is higher in the IQ•SPECT images with normalization of inferior wall tracer uptake following accurate CTAC.

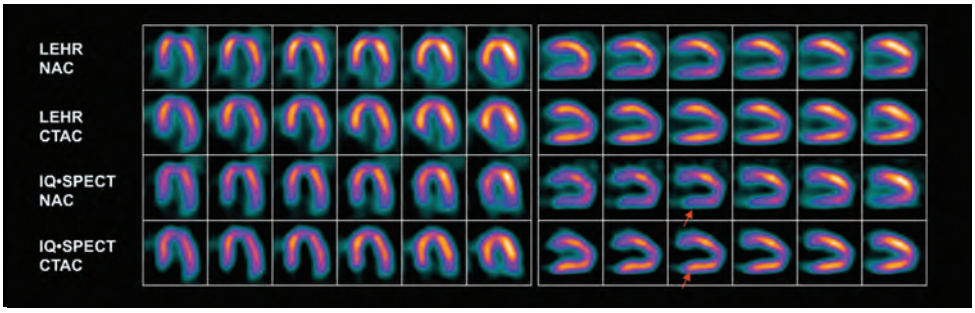


**Figure 3c:** Data courtesy of University of Michigan, Ann Arbor, Michigan, USA.

**Figure 3c:** Horizontal and vertical long axis views of stress MPI of the same patient with the display identical to the short axis shows exaggerated inferior wall attenuation in the uncorrected IQ•SPECT images, which is corrected following CTAC, with normal inferior wall uptake visualized in the corrected images. Note the slightly different orientation of the mitral valve plane in the IQ•SPECT images compared to the LEHR images.

**Study protocol:** Symbia T16; 20 mCi $^{99m}$Tc-Sestamibi stress injection; IQ•SPECT stress study: 17 frames, 9 seconds per frame (total scan time: 4 minutes). LEHR stress study: 32 frames, 24 seconds per frame (total scan time: 14 minutes).

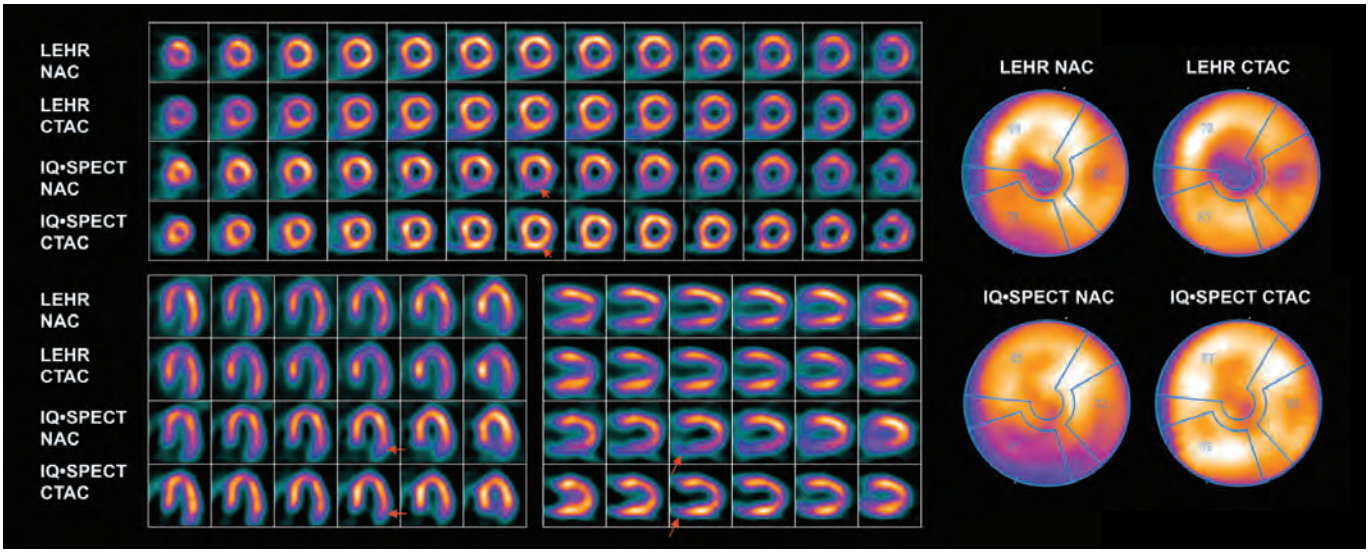


**Figure 4:** Data courtesy of the University of Michigan, Ann Arbor, MI, USA.

**Figure 4:** Above is a comparison of LEHR and IQ•SPECT $^{99m}$Tc-MIBI stress MPI in a normal male without and following CTAC, with the acquisition protocol similar to that of the previous case example. Note the higher inferior wall attenuation levels with IQ•SPECT, which is corrected by CTAC. Also note the posterobasal attenuation (red arrows) in the vertical and horizontal long axis views, which also shows significant improvement in uptake levels following CTAC. Exaggerated posterobasal, as well as inferior wall attenuation correction, is common with IQ•SPECT, but is effectively corrected by CTAC.

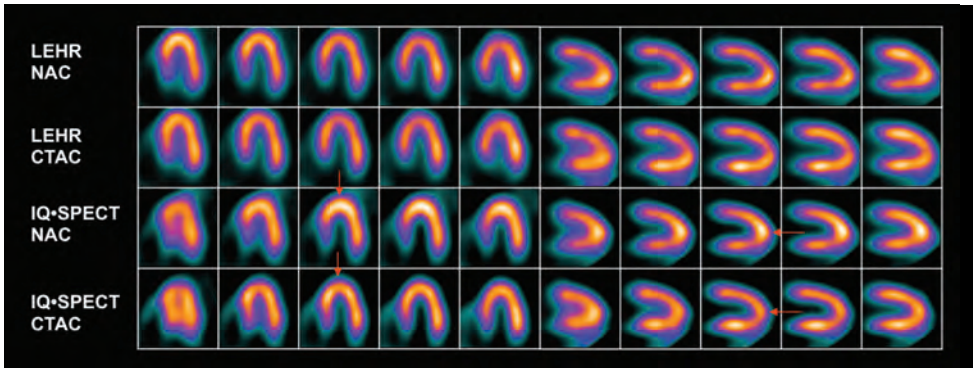


**Figure 5a:** Data courtesy of University of Michigan, Ann Arbor, Michigan, USA.

**Figure 5a:** A $^{99m}$Tc-MIBI stress MPI comparison of LEHR and IQ•SPECT in a 37-year-old female with normal perfusion. Note the hot apex in the uncorrected IQ•SPECT images (red arrows) which normalizes following CTAC. A thick apex with increased uptake is a common finding in the uncorrected IQ•SPECT images both in male and female patients due to the non-uniform attenuation levels of apex and the lateral and septal walls. Such a hot apex effect is usually decreased following attenuation correction and renormalization of the uptake throughout the entire LV myocardium.

**Study protocol:** Symbia T16; 20 mCi $^{99m}$Tc-Sestamibi stress injection; IQ•SPECT stress study: 17 frames, 9 seconds per frame (total scan time: 4 minutes); LEHR stress study: 32 frames, 24 seconds per frame (total scan time: 14 minutes); low-dose CT-based attenuation correction.

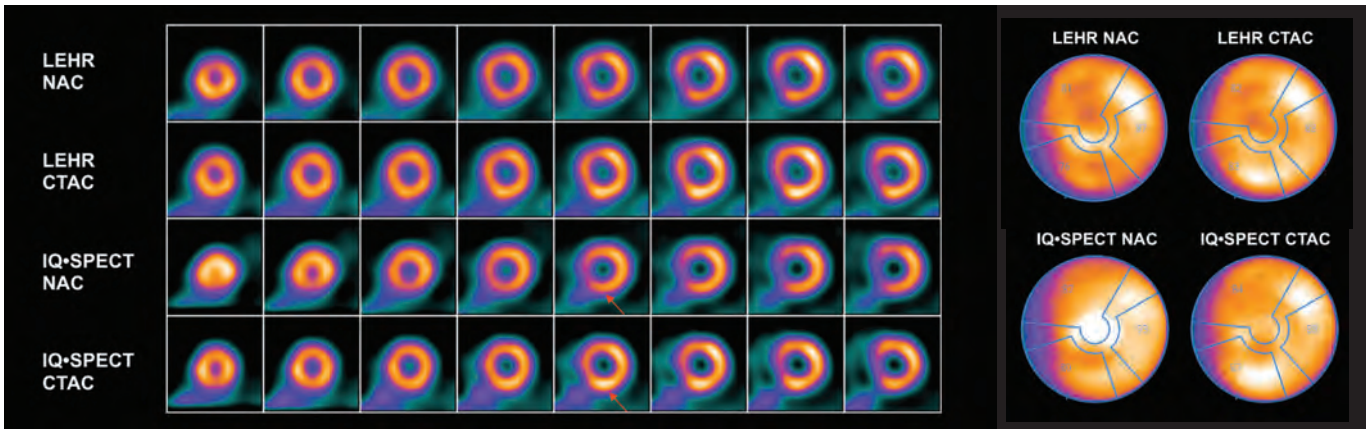


**Figure 5b:** Short axis views of the same patient show slight inferior wall attenuation, which is corrected in the CTAC images. Despite this patient being female, there is very little anterior wall attenuation.

**Figure 5b:** Data courtesy of the University of Michigan, Ann Arbor, MI, USA.

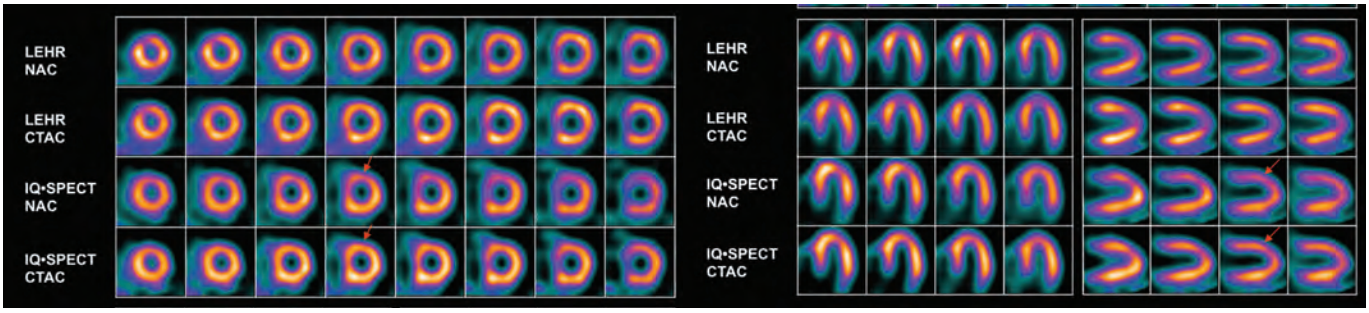


**Figure 6:** Data courtesy of University of Michigan, Ann Arbor, Michigan, USA.

**Figure 6:** A $^{99m}$Tc-MIBI stress MPI in a 59-year-old female patient shows normal perfusion at peak stress. LEHR and IQ•SPECT images show comparable image quality and tracer distribution. Note the predominant anterior wall attenuation (red arrows), which is corrected following CTAC. It is important to note the higher level of anterior wall attenuation with IQ•SPECT without attenuation correction (non-AC). However, post-CTAC IQ•SPECT images show perfect correction of anterior wall attenuation effects.

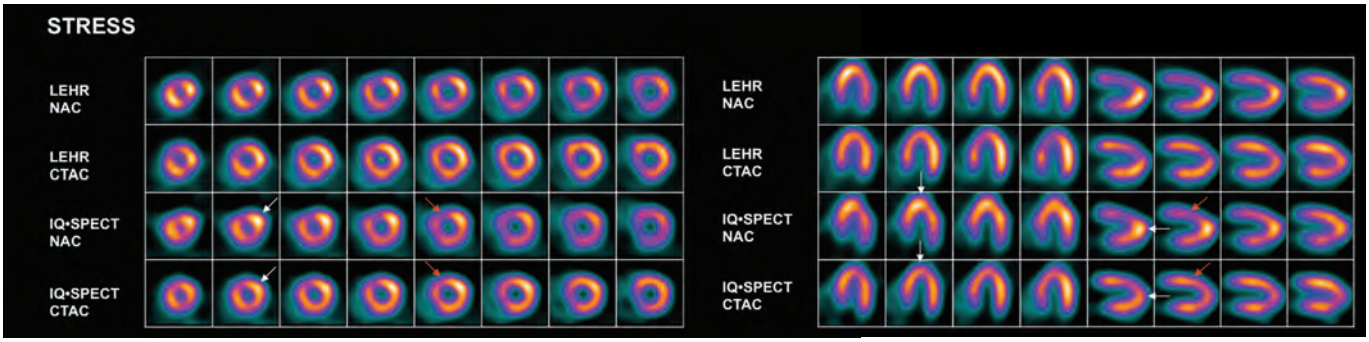


**Figure 7a:** Data courtesy of University of Michigan, Ann Arbor, Michigan, USA.

**Figure 7a:** A $^{99m}$Tc-MIBI stress-rest MPI study was performed on a 48-year-old female patient using LEHR and IQ•SPECT. A comparison of stress LEHR and IQ•SPECT images (non-AC and with CTAC) shows a combination of anterior wall attenuation correction along with thick hot apex predominantly in the IQ•SPECT images, but also, to a lesser extent, in the LEHR images. Anterior wall attenuation (red arrows) in uncorrected images is well-corrected following CTAC. Apical thickness and increased apical uptake in non-AC images (white arrows) is pronounced in the uncorrected IQ•SPECT images but is normalized following CTAC. Short axis IQ•SPECT slices toward the apex show the combination of increased uptake at the apex and adjacent anterolateral wall (white arrow), along with attenuation effect on the anterior wall, which leads to distortion of the shape of the LV in short axis. This is, however, completely corrected following CTAC. The combination of attenuation effects along with apical thickening and increased tracer uptake in the uncorrected IQ•SPECT should be carefully considered during the interpretation of uncorrected data and compared with the CTAC data.

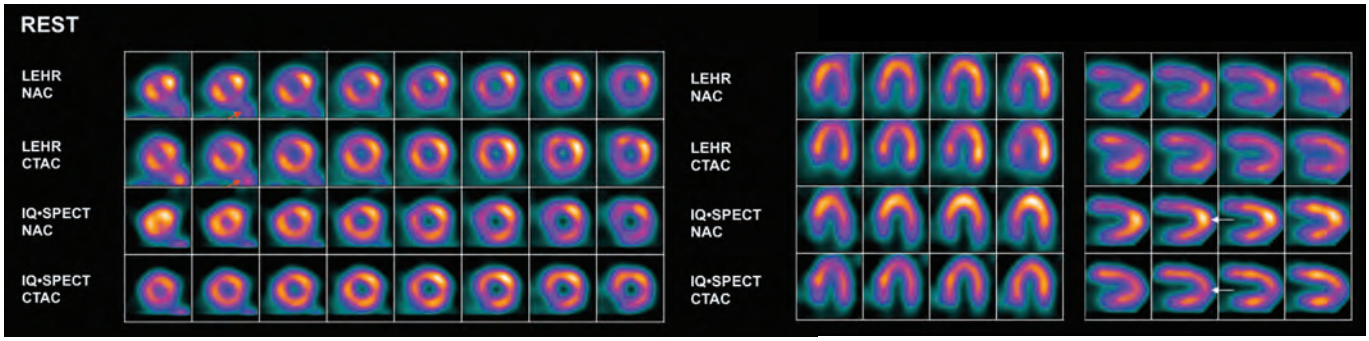


**Figure 7b:** A comparison of rest images for the same patient also demonstrates the effect of hot apex and subsequent normalization following CTAC (white arrows). However, of note is the tracer uptake in the gut just inferior and adjacent to the infero-lateral wall, which is accentuated following attenuation correction (red arrows). In this case, the effect is more pronounced in the LEHR images. However, IQ•SPECT images tend to also show increased gut uptake following CTAC. This potential of AC-dependent increased gut uptake and its contribution to inferior and inferolateral wall uptake should be considered during interpretation. A review of the rotating maximum intensity projection (MIP) of the acquisition is often helpful to determine the extent of gut uptake and estimate its contribution to the inferior wall uptake.

**Figure 7b:** Data courtesy of University of Michigan, Ann Arbor, Michigan, USA.

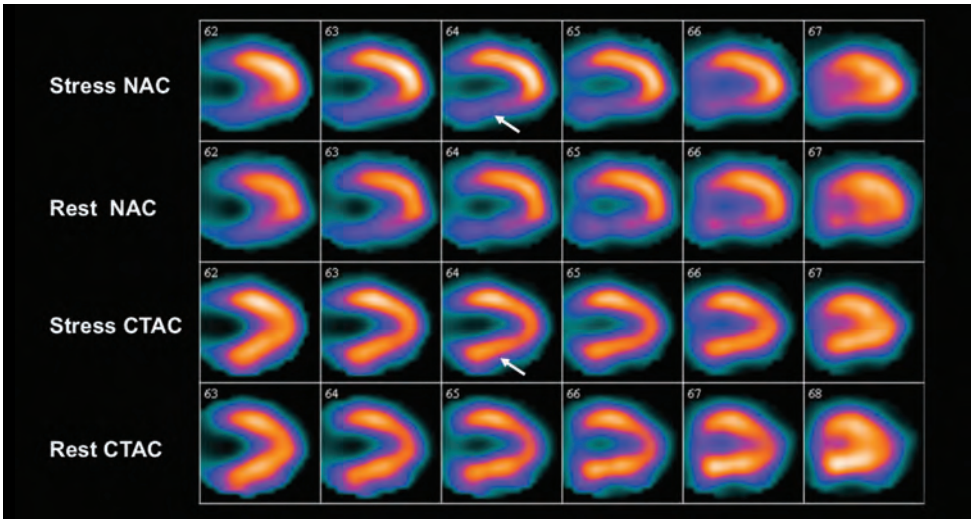


**Figure 8:** Data courtesy of Hopital de la Cite de la Sante de Laval, Canada.

**Figure 8:** Above is a low-dose IQ•SPECT study with inferior wall attenuation corrected by CTAC in IQ•SPECT using low-dose protocol with a 10 mCi sestamibi stress injection and 6-minute acquisition. A 54-year-old female (110 lb/50 kg) was referred for atypical chest pain. The study shows normal perfusion with inferior and posterobasal wall attenuation, which is corrected with CTAC.

Similar normal patterns with IQ•SPECT related to attenuation effects and enhanced apical tracer uptake in uncorrected images are also visualized with $^{201}$Thallium myocardial perfusion imaging using IQ•SPECT.

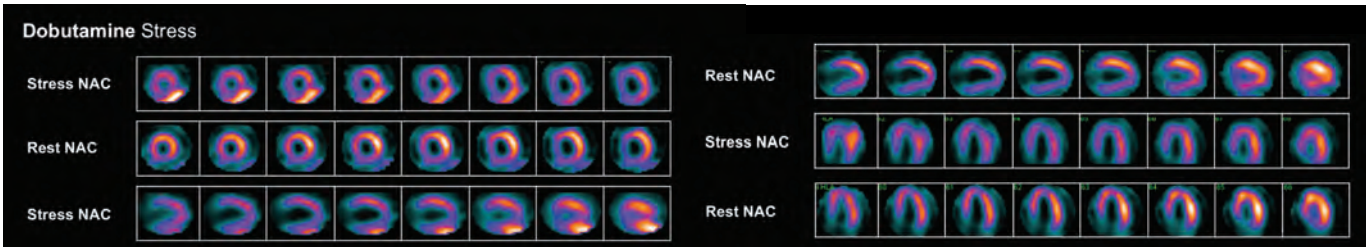


**Figure 9a:** Data courtesy of Hopital de la Cite de la Sante de Laval, Canada.

**Figure 9a:** An 82-year-old male with long-standing diabetes treated by insulin presented with typical angina and dyspnea. There was history of past allergic reaction to aminophylline. A $^{99m}$Tc MIBI myocardial perfusion IQ•SPECT study was performed using pharmacologic stress test with dobutamine. An 80% maximal predicted heart rate response was achieved after 1 mg atropine. No ST-T changes were observed on the EKG during dobutamine stress.

Non-AC stress and rest images show very high liver and gastric activity in the stress study related to the dobutamine stress, which makes interpretation of inferior wall uptake difficult. The rest study shows slightly reduced inferior wall uptake, which may be related to attenuation effect, but, without a clear inferior wall uptake assessment in the stress study, it is difficult to characterize the uptake.

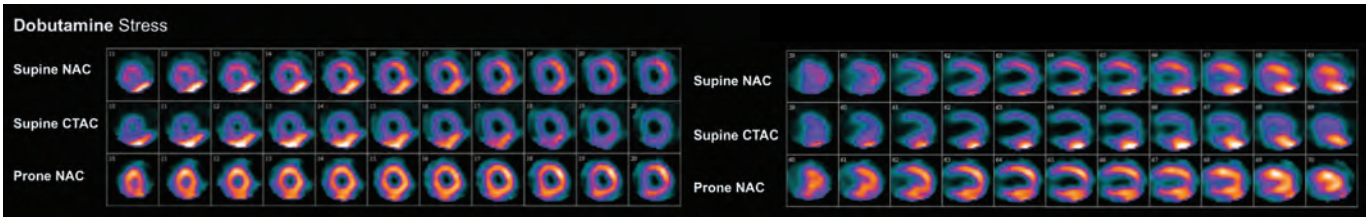


**Figure 9b:** Data courtesy of Hopital de la Cite de la Sante de Laval, Canada.

**Figure 9b:** The patient also underwent a stress IQ•SPECT study in a prone position with a separately performed CT immediately after completion of the supine stress study. Supine non-AC and CTAC images, along with non-AC prone images, are displayed in short axis and the vertical long axis (VLA). Supine images show high hepatic and gastric uptake of tracer, which overlaps the inferior wall, making inferior wall interpretation difficult. Following the CTAC of the supine images, there is further accentuation of the subdiaphragmatic uptake and artificially decreased anterior wall and septal uptake due to renormalization. However, the prone images, even without CTAC, as shown in this image, show homogenous distribution of tracer throughout the LV myocardium with normal appearance of the inferior wall. The study was interpreted as normal. This example clearly demonstrates the value of prone imaging in specific situations, especially related to the interference of inferior wall attenuation and hepatic gastric and bowel uptake with interpretation.

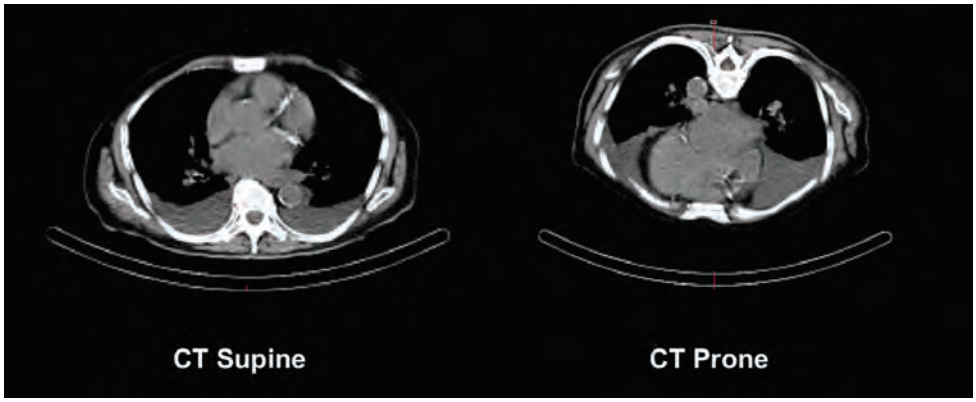


**Figure 9c:** Data courtesy of Hopital de la Cite de la Sante de Laval, Canada.

**Figure 9c:** CT slices in both supine and prone positions for the same patient show a significant amount of pleural fluid with shifting of fluid to the dependent part of the thorax between the supine and prone positions. The shift of the ventricles toward the chest wall in the prone position is also well-visualized on the prone CT image, which reflects the absence of hepatic and gastric interference. CT images also show diffuse three vessel calcification.

The SPECT/CT study was interpreted as normal. The final diagnosis was global cardiac insufficiency related to atrial fibrillation without significant coronary artery disease (CAD). Clinical follow-up after four months was uneventful.

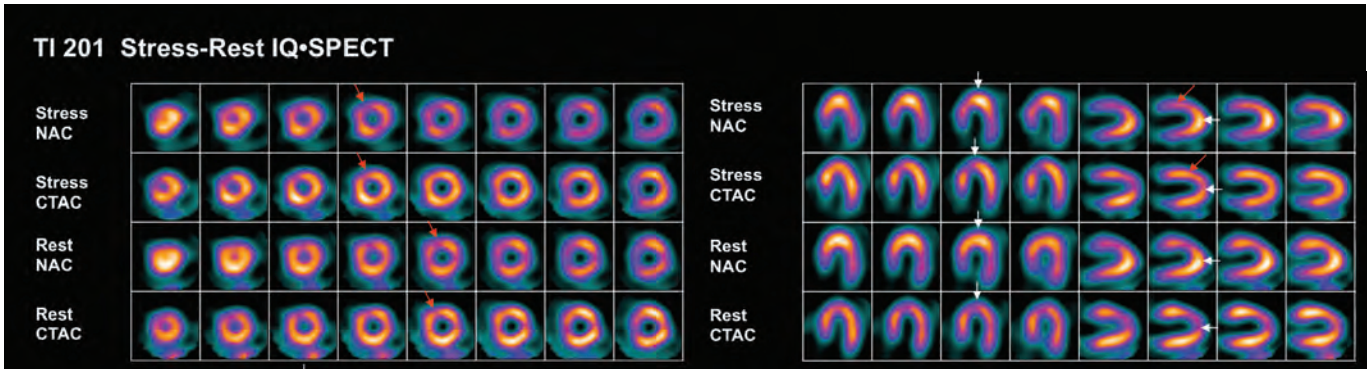


**Figure 10:** Data courtesy of Hopital de la Cite de la Sante de Laval, Canada.

**Figure 10:** A 71-year-old female underwent stress-rest $^{201}$Tl MPI using IQ•SPECT. A comparison of stress and rest images without and with CTAC shows the typical patterns of anterior wall attenuation (red arrows), which is well-corrected following CTAC. Note the apical thickness and increased apical uptake in both uncorrected stress and rest images, which is well-corrected following CTAC (white arrows). The hot apex in uncorrected images following CTAC and renormalization of tracer uptake throughout the LV myocardium shows slight apical thinning in the CTAC images. Exaggerated apical thinning following CTAC is a regular pattern both in LEHR and IQ•SPECT images.

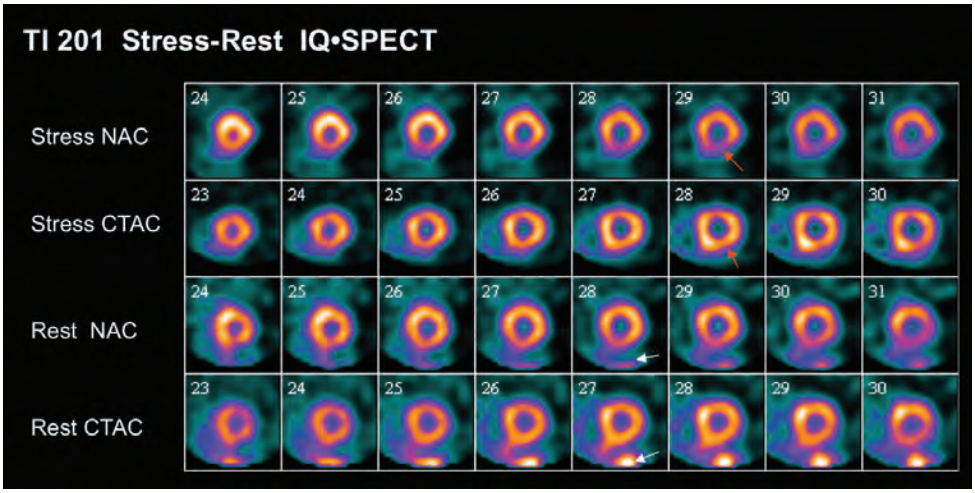


**Figure 11:** Data courtesy of Atrium Medical Center, Heerlen, The Netherlands.

**Figure 11:** $^{201}$Thallium stress-rest IQ•SPECT short axis views of a 56-year-old male patient show inferior wall attenuation (red arrows), which is corrected after CTAC. Note the tracer uptake in the gut in the rest images, particularly the increase in gut uptake following attenuation correction (white arrows). Such increase in stomach and intestinal uptake following attenuation correction is common in IQ•SPECT and needs to be considered when interpreting inferior wall uptake.

## IQ•SPECT: clinical studies supporting the relative equivalence of IQ•SPECT and LEHR acquisitions

A group from the University of Michigan compared 4-minute IQ•SPECT MPI with conventional LEHR acquisition performed in 15-20 minutes.[a] A total of 110 patients referred for myocardial perfusion imaging underwent a $^{99m}$Tc-MIBI stress-only or stress-rest single-day protocol MPI study, performed initially with parallel-hole collimation using a Symbia T16 SPECT/CT and subsequently with IQ•SPECT, employing **SMART**ZOOM collimators and cardio-centric orbits on the same system without significant delay between studies. Low-dose CT for attenuation correction was acquired initially. A standard LEHR SPECT/CT was performed over 180° orbits at 3° increments for 15-20 seconds per view into 128 x 128 matrices and 4.8 mm pixels. The study time was 15-20 minutes. IQ•SPECT images were acquired over a 208° cardio-centric orbit with 17 views per detector for 9 seconds per view to 128 x 128 matrices and 4.80 mm pixels. The total study time was 4 minutes. Both LEHR and IQ•SPECT images were corrected for attenuation using initially acquired low-dose CT. Normal databases were created from 30 low-likelihood normal males and 22 low-likelihood females. Standard 17 segment scoring and blackout polarmap analyses were employed using Corridor4DM™ software. Image quality was similar between LEHR and IQ•SPECT for most patients. Among 13 low-likelihood normals not included in the normal databases, 11 were normal with IQ•SPECT and 12 were normal with LEHR. Fourteen patients were determined to have coronary artery disease in both the LEHR and IQ•SPECT studies. The summed stress scores (SSS) were similar to IQ•SPECT and LEHR (13.9 ± 10.2 as 12.4 ± 11.4, respectively). Defect sizes were also similar between the two acquisitions. Angiographic correlation was also similar, with a trend of increased sensitivity with IQ•SPECT (12 vs. 8 true positives by SSS). Overall, a quantitative analysis of IQ•SPECT and LEHR showed comparable image quality, normalcy rates, and sensitivity.

The same group presented another abstract[2] comparing LEHR and IQ•SPECT acquisition with CTAC in 54 patients, 37 of which were low-likelihood normals. Seven patients underwent coronary angiography. Images were scored from 0 (unacceptable) to 4 (excellent). Image quality was similar for the two methods, with an average score of 3.11 for LEHR and 3.21 for IQ•SPECT. Thirty-three studies were rated of good or excellent quality with LEHR and 36 studies with IQ•SPECT. Assessments of normalcy were very similar with values of 91% for LEHR and 97% with IQ•SPECT. Angiographic correlations performed in 7 patients were almost identical. Studies in patients without significant stenoses (< 50%) were normal for both LEHR and IQ•SPECT. Patients with higher stenosis severity on angiography showed consistently higher SSS with IQ•SPECT as compared to LEHR.

## IQ•SPECT clinical examples: coronary artery disease

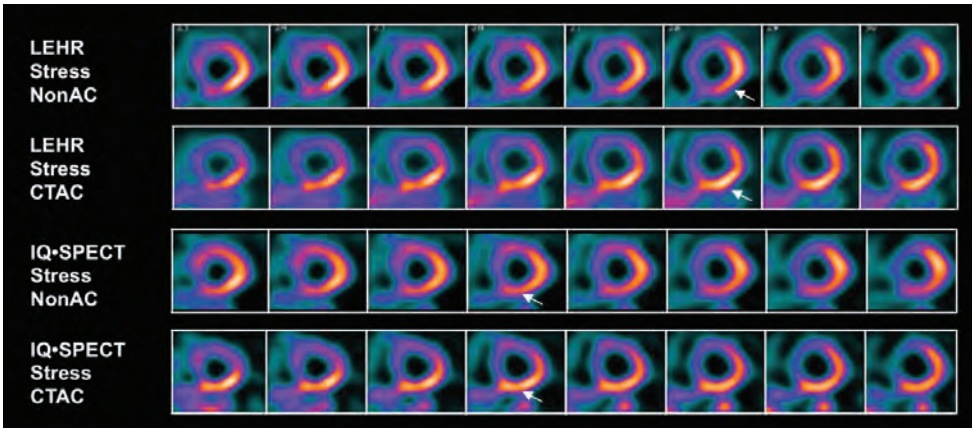


**Figure 12a:** Data courtesy of the University of Michigan, Ann Arbor, MI, USA.

**Figure 12a:** A 78-year-old man with anginal pain underwent $^{99m}$Tc MIBI stress-rest MPI using both LEHR and IQ•SPECT with low-dose CTAC.

**Study protocol:** Symbia T16; Dose: stress–21.5 mCi 30-minute post-injection delay, rest–42 mCi; low-dose, free-breathing CT for attenuation correction.

The acquisition parameters of the LEHR and IQ•SPECT were as follows:

**LEHR stress:** 32 frames, 22 seconds per frame (total acquisition time 13 minutes)

**LEHR rest:** 32 frames, 11 seconds per frame (total acquisition time 7 minutes)

**IQ•SPECT stress:** 17 frames, 9 seconds per frame (total acquisition time 4 minutes)

**IQ•SPECT rest:** 17 frames, 9 seconds per frame (total acquisition time 4 minutes)

A comparison of LEHR and IQ•SPECT short axis stress images shows a severe perfusion defect in the anterior wall and septum. The lateral wall also shows moderate perfusion defect better defined on CTAC images. The inferior wall shows improved uptake in the CTAC images, suggestive of attenuation. The LV cavity appears dilated, suggestive of severe CAD. Note the comparable extent and intensity of perfusion defect with IQ•SPECT compared to LEHR both in non-AC and CTAC images.

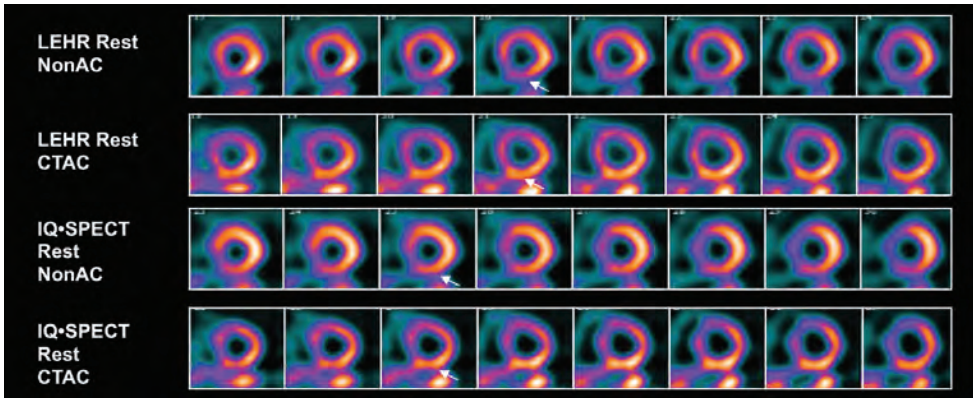


**Figure 12b:** Data courtesy of the University of Michigan, Ann Arbor, MI, USA.

**Figure 12b:** A rest study comparing LEHR and IQ•SPECT short axis images in the same patient shows significant increase in anterior and anteroseptal segments, suggesting reversible ischemia. Note the inferior wall attenuation, which is corrected following CTAC and also causes a slight increase in the intensity of the gut uptake in the corrected images. Due to renormalization of the LV myocardial uptake, anterior wall uptake is slightly lower in the corrected IQ•SPECT slices compared to the uncorrected. The variation of uptake intensity following CTAC due to renormalization is of consideration during comparative interpretation of non-AC and CTAC images.

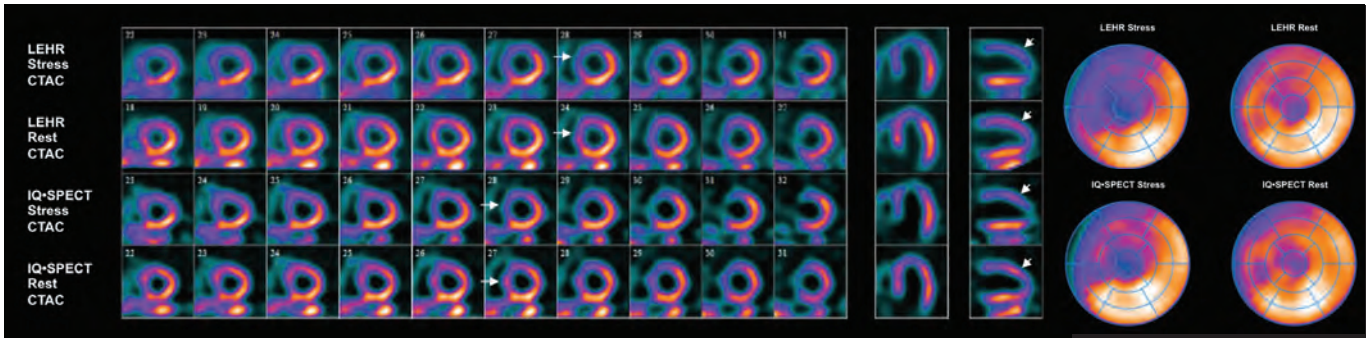


**Figure 12c:** Data courtesy of the University of Michigan, Ann Arbor, MI, USA.

**Figure 12c:** Stress and rest short axis slices displayed for both attenuation-corrected LEHR and IQ•SPECT images show severe but reversible ischemia in anterior wall and septum left anterior descending artery (LAD) territory, along with moderate reversible lateral wall ischemia (left circumflex).

A CT calcium score was performed as part of the SPECT/CT procedure, which revealed extensive calcification of the LAD with significant calcification in the right coronary artery (RCA) and left circumflex.

The patient was subjected to coronary angiography, which revealed 90% ostial stenosis in the LAD with another 70% stenosis at mid-LAD at the bifurcation of D2 (second diagonal). The left circumflex was the dominant vessel with 30% ostial stenosis and mid-20% stenosis. The right coronary artery was non-dominant with a mid-90% stenosis.

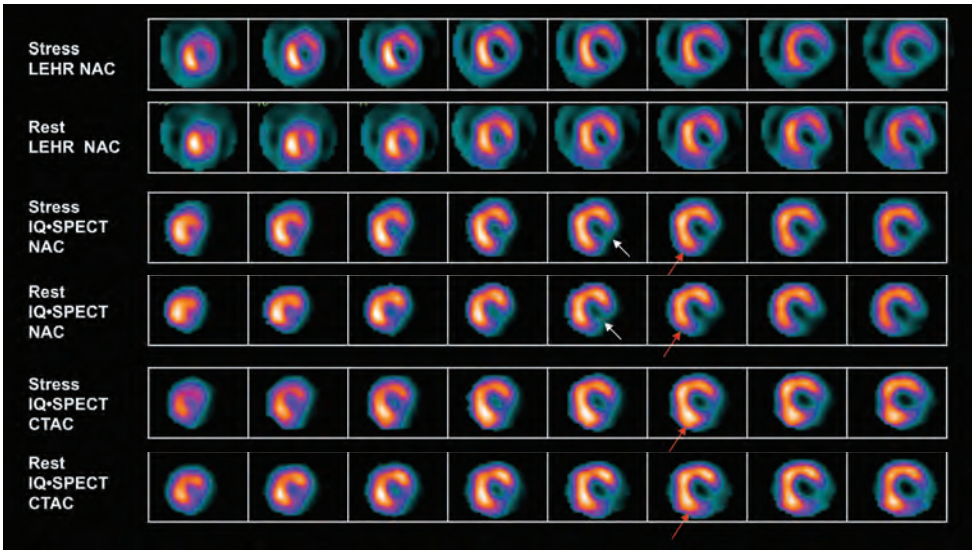


**Figure 13a:** Data courtesy of Hopital de la Cite de la Sante de Laval, Canada.

**Figure 13a:** A $^{99m}$Tc-MIBI stress-rest MPI was performed using LEHR and IQ•SPECT in a patient with inferolateral infarction. A fixed inferolateral defect in uncorrected and corrected short axis images reflects large inferolateral infarction without evidence of peri-infarct ischemia. Note the improvement in inferoseptal uptake in the attenuation-corrected images.

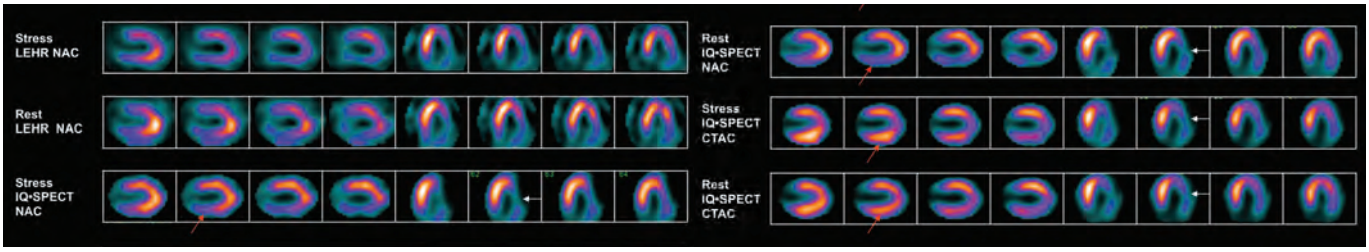


**Figure 13b:** Data courtesy of Hopital de la Cite de la Sante de Laval, Canada.

**Figure 13b:** Vertical and horizontal long axis views in the same patient show a fixed lateral and inferolateral wall defect (white arrows) both in non-AC and CTAC images. However, the posterobasal defect in uncorrected IQ•SPECT stress and rest images (red arrows) shows significant improvement following CTAC, which suggests significant posterobasal attenuation effect. This study demonstrates the advantage of CTAC in the presence of perfusion defects to improve specificity, as well as correctly define the extent and intensity of ischemia.

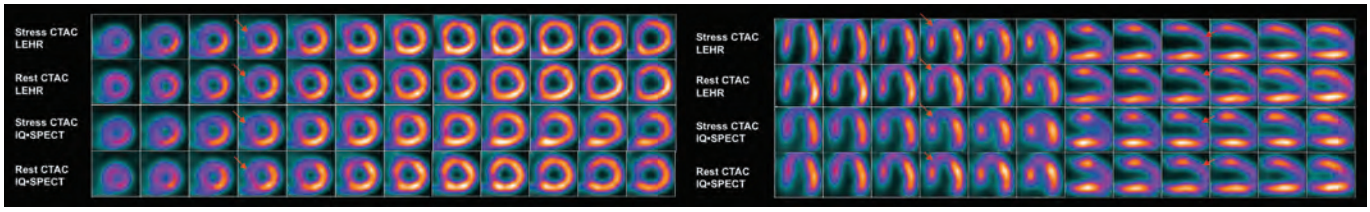


**Figure 14a:** A 65-year-old male patient (225 lb/102 kg) with shortness of breath on exertion, hypercholesterolemia, and a family history of coronary artery disease underwent $^{99m}$Tc-sestamibi myocardial perfusion imaging. The standard LEHR acquisition and an IQ•SPECT acquisition were performed at rest and following treadmill stress. A CT calcium score was performed prior to the SPECT study on a Symbia T6. CT attenuation-corrected IQ•SPECT stress images show severe ischemia in the anterior wall, septum and apex with significant reversibility in the resting images. The attenuation-corrected LEHR acquisitions show a similar extent of ischemia and reversibility. The LV cavity size appears similar in both studies. Note the increased severity of perfusion defect in the stress IQ•SPECT images (vertical long axis slices) compared to that of LEHR.

**Figure 14a:** Data courtesy of the University of Michigan, Ann Arbor, MI, USA.

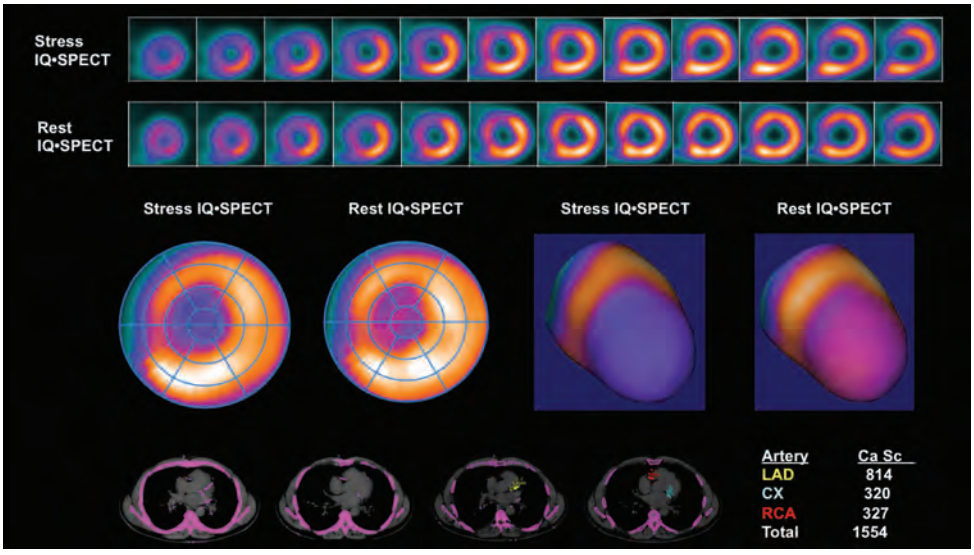


**Figure 14b:** Data courtesy of the University of Michigan, Ann Arbor, MI, USA.

**Figure 14b:** The calcium score study in the same patient shows a total calcium score of 1554 with extensive calcification in all three vessels, with maximum involvement of LAD.

**Study protocol:** Symbia T6; 27 mCi $^{99m}$Tc-Sestamibi stress injection, 50 mCi $^{99m}$Tc-Sestamibi rest injection after 2 hours.

**IQ•SPECT stress study:** 36 frames, 10 seconds/frame

**LEHR stress study:** 32 frames, 41 seconds/frame

**IQ•SPECT rest study:** 36 frames, 3 seconds/frame

**LEHR rest study:** 32 frames, 12 seconds/frame

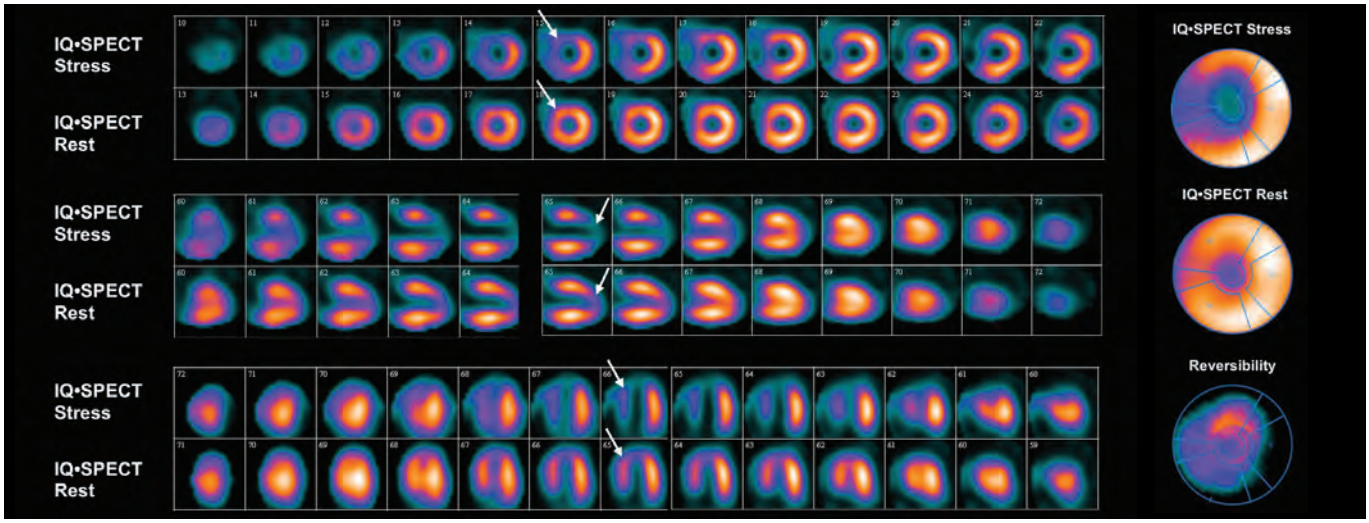


**Figure 15a:** Data courtesy of Hopital de la Cite de la Sante de Laval, Canada.

**Figure 15a:** A 67-year-old woman presented with atypical chest pain. An IQ•SPECT study was performed at rest and, using pharmacological stress, showed severe and extensive ischemia in the anterior wall and septum (LAD territory). Post-stress transient ischemic dilatation suggests advanced multi-vessel disease. The patient was referred for coronary angiography.

**Study protocol:** 25 mCi $^{99m}$Tc-Sestamibi stress injection; 17 frames, 9 second/frame, 4 minutes total IQ•SPECT acquisition; low-dose, free-breathing CT for attenuation correction.

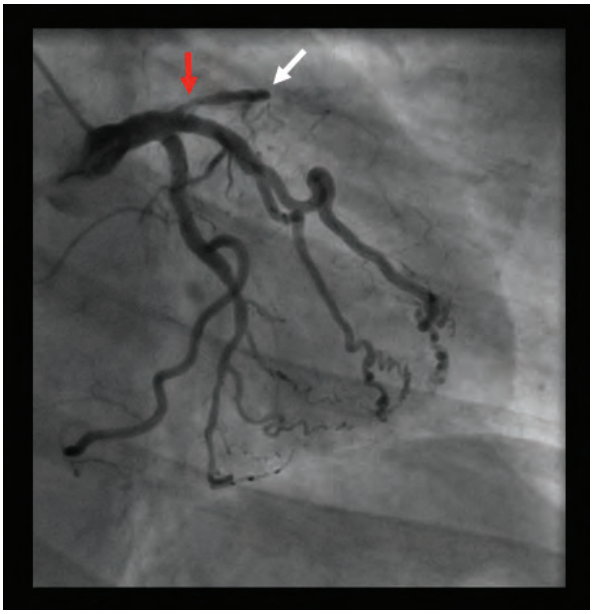

**Figure 15b:** Data courtesy of Hopital de la Cite de la Sante de Laval, Canada.

**Figure 15b:** Coronary angiography of the same patient showed chronic occlusion of the mid-LAD (white arrow), as well as a 50% stenosis of the proximal LAD (red arrow). The patient underwent bypass surgery after a failed angioplasty attempt.

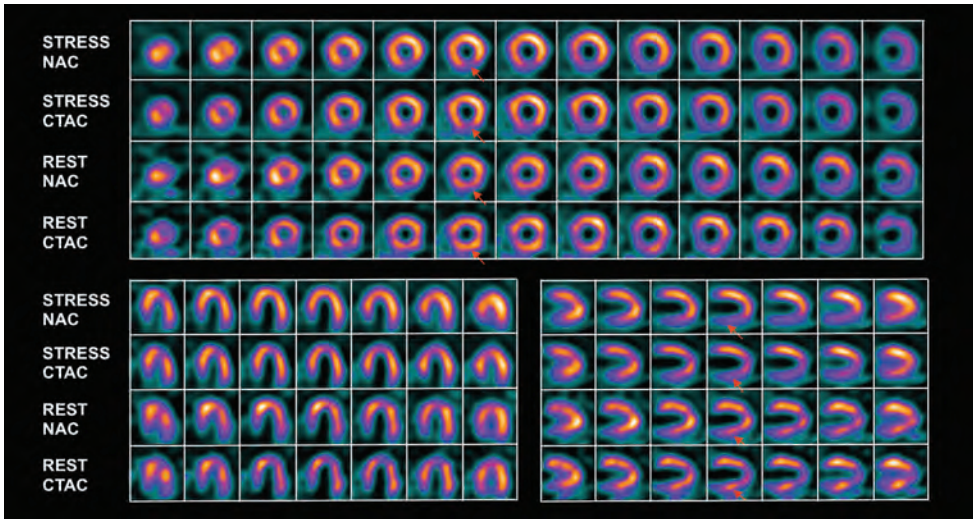


**Figure 16:** Data courtesy of the University of Sherbrooke, Sherbrooke, Quebec, Canada.

**Figure 16:** A $^{99m}$Tc-MIBI stress-rest IQ•SPECT MPI was performed with low-dose CTAC in a patient with suspected CAD. Non-AC stress images show inferior wall perfusion defect, which persists following CTAC, although the intensity is reduced. There is significant improvement in inferior wall uptake both in non-AC and CTAC rest images, suggesting reversible inferior wall ischemia. CTAC, in this example, improves diagnostic confidence to identify a small inferior wall defect as true ischemia and not a pure attenuation effect.

**Study protocol:** Symbia T6; Dose: Stress–20 mCi, Rest–7 mCi $^{99m}$Tc-MIBI; IQ•SPECT: Stress 17 frames/9 seconds per frame (scan time: 4 minutes), Rest: 17 frames/25 seconds per frame (scan time 8.5 minutes).

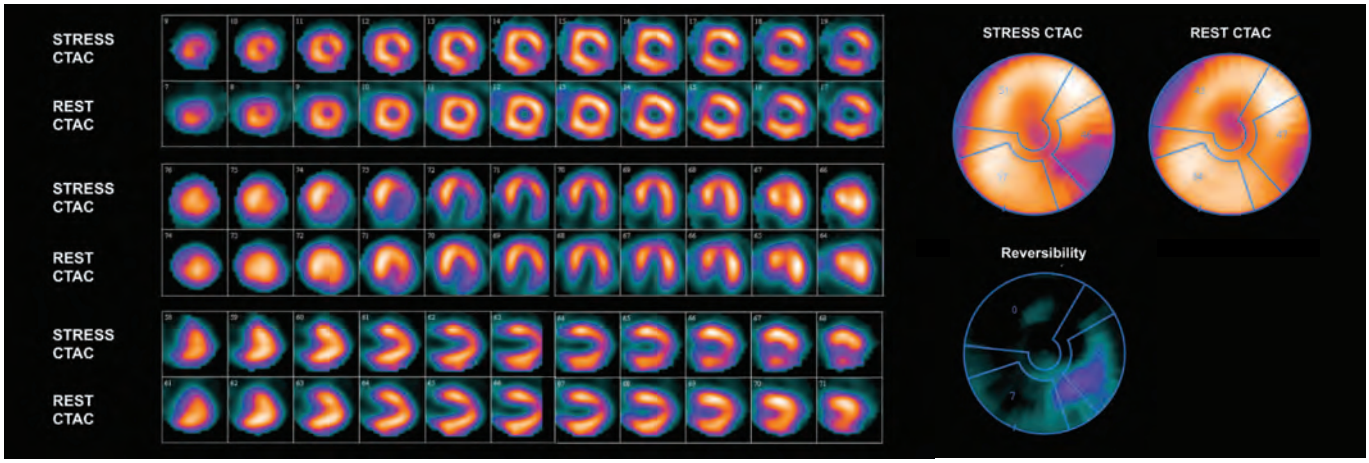


**Figure 17a:** Data courtesy of the University of Sherbrooke, Sherbrooke, Quebec, Canada.

**Figure 17a:** Single vessel disease: a 65-year-old female with exertion-induced chest pain and hypertension was referred for an MPI study to evaluate for inducible ischemia. IQ•SPECT performed at rest and with pharmacological stress shows reversible ischemia in the inferolateral wall. The rest of the LV myocardium showed normal perfusion. The patient subsequently underwent coronary angiography.

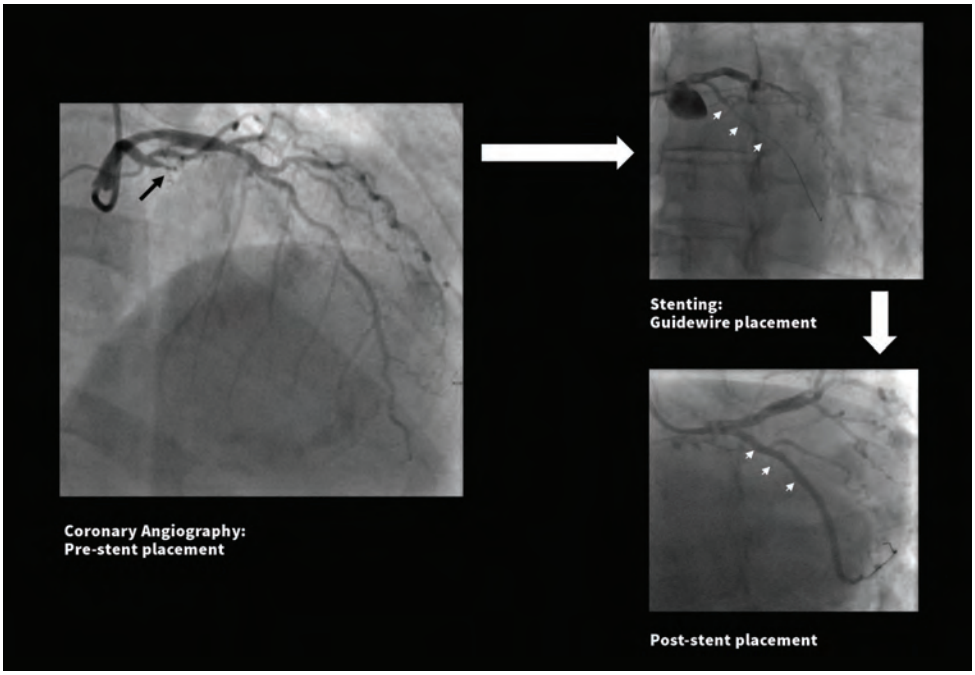


**Figure 17b:** Data courtesy of Hopital de la Cite de la Sante de Laval, Canada.

**Figure 17b:** A coronary angiography for the same patient shows single 95% stenosis of the mid left circumflex artery (black arrow), which correlates well with IQ•SPECT findings. The patient underwent stenting of the lesion. Coronary flow was completely restored after the successful placement of two stents (white arrows).

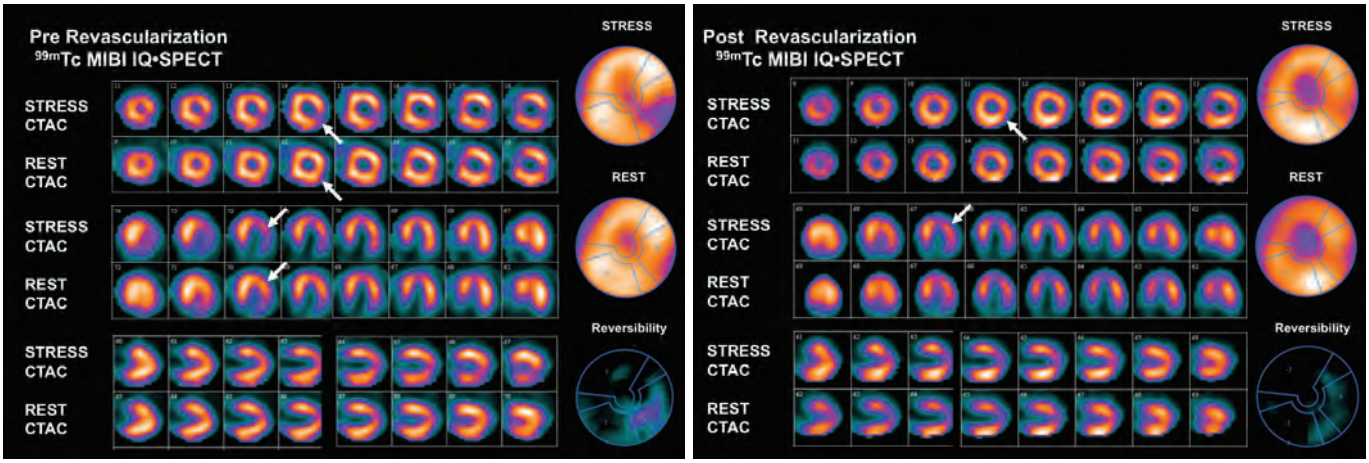


**Figure 17c:** Data courtesy of Hopital de la Cite de la Sante de Laval, Canada.

**Figure 17c:** A follow-up MPI study was performed for atypical chest pain after revascularization, which shows normalization of the reversible defect of the inferolateral wall (white arrows). Attenuation corrected pre- and post-stenting studies (6-month interval between MPI studies) shows significant improvement in the inferolateral defect with normal perfusion throughout the rest of the LV myocardium. Note the prominent apical thinning in the post-stent IQ•SPECT study, which is a common post-attenuation correction finding in IQ•SPECT studies.

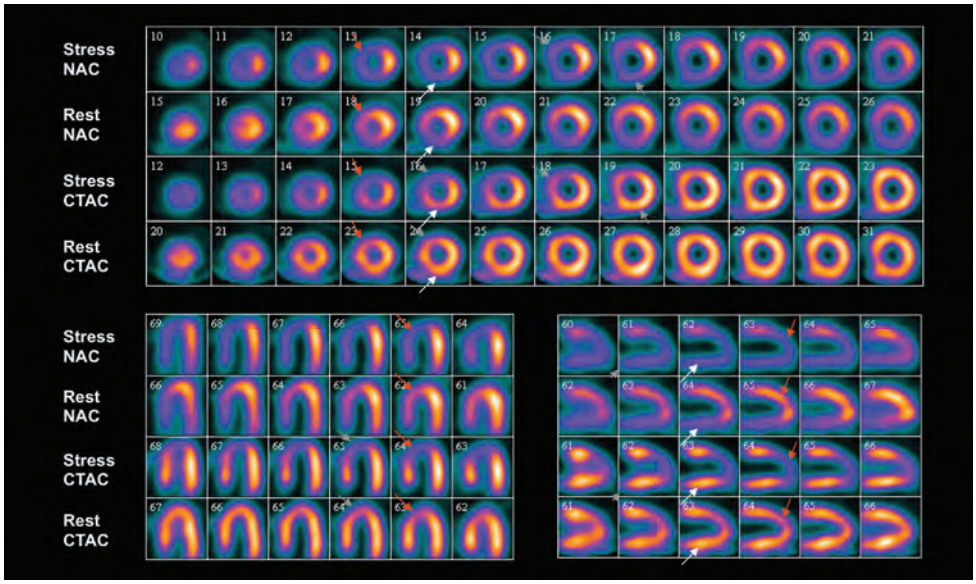


**Figure 18:** Data courtesy of BWZK Hospital, Koblenz, Germany.

**Figure 18:** A $^{99m}$Tc-MIBI stress-rest MPI performed using IQ•SPECT shows reversible ischemia in the anterior wall and septum (LAD territory—red arrows). The inferior wall defect seen in both non-AC stress and rest images shows improvement in uptake in the CTAC images, suggesting diaphragmatic attenuation (white arrows). CTAC defines the true extent of LV ischemia and helps define the LAD territory as the only ischemic segment.

**Study protocol:** Symbia T6; 20.2 mCi $^{99m}$Tc-Sestamibi stress 6.7 mCi rest.

**IQ•SPECT stress study:** 17 frames, 14 seconds per frame (total scan time: 4.7 minutes)

**IQ•SPECT rest study:** 17 frames, 30 seconds per frame (total scan time: 9 minutes)

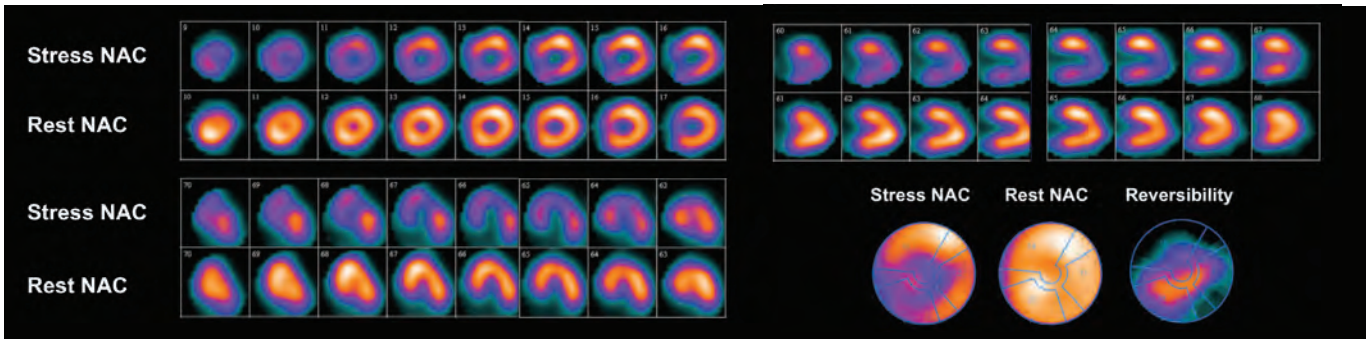


**Figure 19a:** Data courtesy of Hopital de la Cite de la Sante de Laval, Canada.

**Figure 19a:** This clinical example is of a 71-year-old female with multiple CAD risk factors like smoking, hypertension, and a family history of CAD. She underwent a dipyridamole stress IQ•SPECT myocardial perfusion study for unstable angina. A non-AC stress perfusion study shows widespread apical, peri-apical, septal, inferior, and inferoseptal ischemia with transient LV dilation, consistent with multi-vessel CAD. The rest study suggests complete reversibility of all ischemic segments. The patient was referred for urgent coronary angiography.

Data courtesy of Hopital de la Cite de la Sante de Laval, Canada.

**Figure 19b:** Coronary angiography of the patient described above demonstrated severe stenosis in the proximal LAD, left circumflex, and mid-RCA. The patient was referred for surgical revascularization.

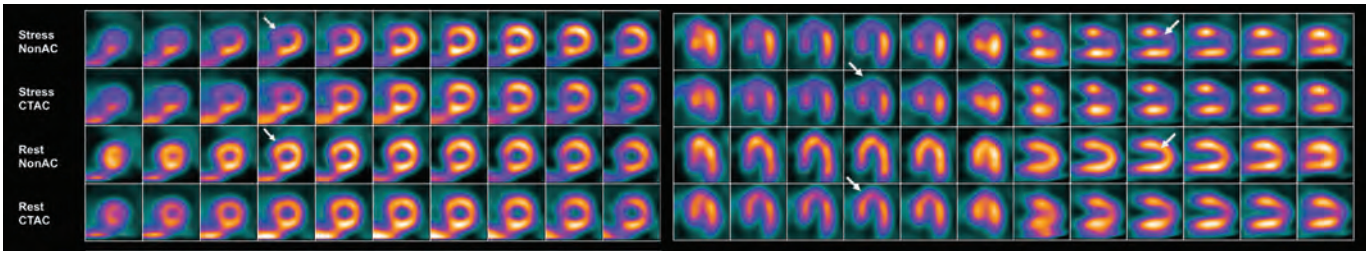


**Figure 20a:** Data courtesy of University of Sherbrooke, Sherbrooke, Quebec, Canada.

**Figure 20a:** A 77-year old female with anginal symptoms underwent $^{99m}$Tc-MIBI IQ•SPECT with pharmacological stress and at rest. Study shows large reversible defect in the apex, adjacent anterior wall, and septum, suggestive of moderate reversible ischemia in distal LAD territory.

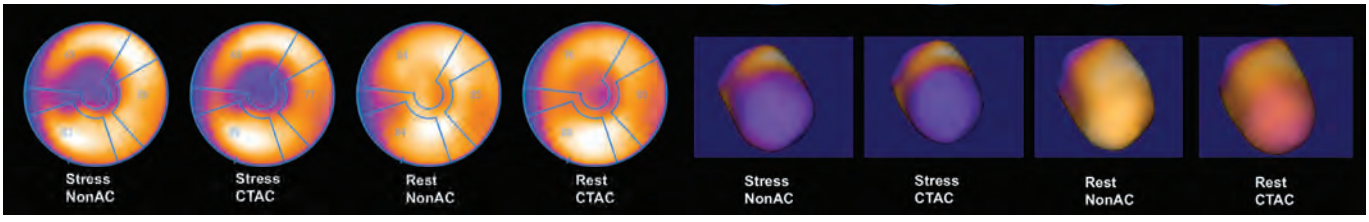


**Figure 20b:** Data courtesy of University of Sherbrooke, Sherbrooke, Quebec, Canada.

**Figure 20b:** Polar plot and volume rendered images of the left ventricle of the patient described above demonstrate the severity of the ischemia of the patient above in the apex and adjacent anterior wall and septum and the complete reversibility at rest. The patient was referred for coronary angiography.

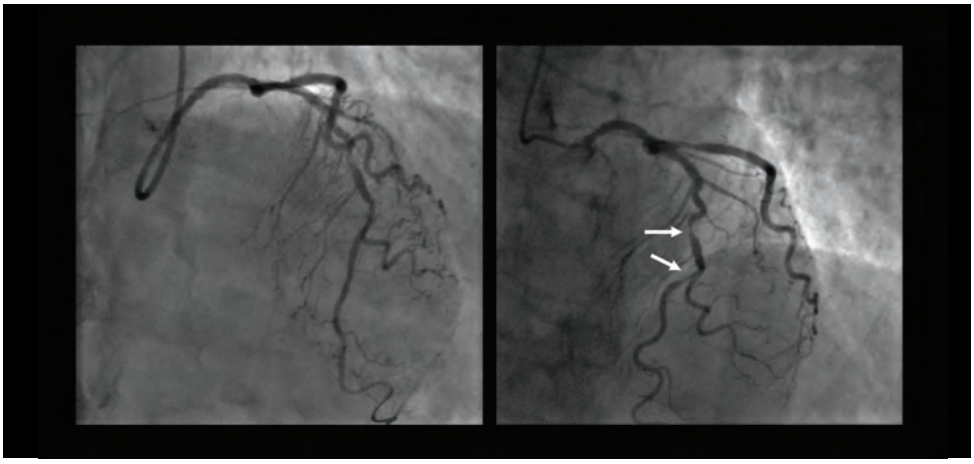

**Figure 20c:** Data courtesy of University of Sherbrooke, Sherbrooke, Quebec, Canada.

**Figure 20c:** Coronary angiography shows two sequential stenoses (80%) at mid-LAD level.

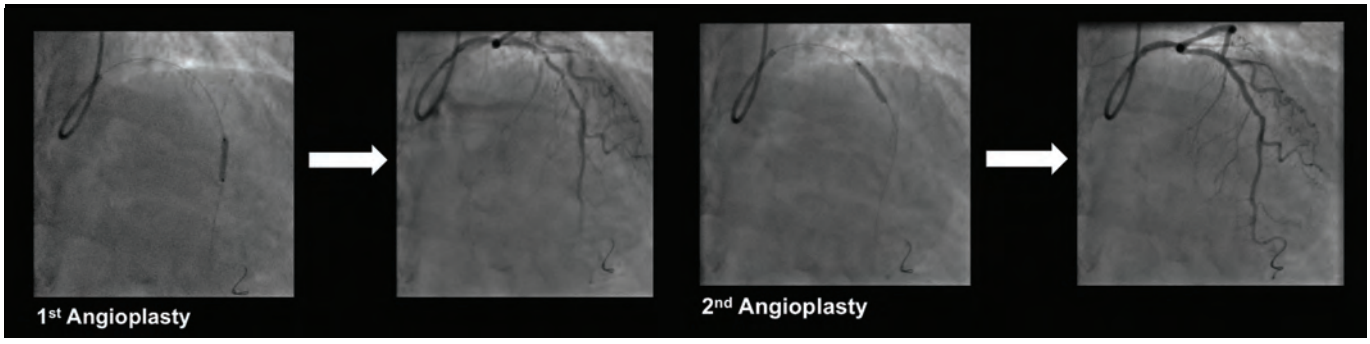


**Figure 20d:** Both mid-LAD lesions were treated with angioplasty and stenosis with complete restoration of flow.

**Figure 20d:** Data courtesy of University of Sherbrooke, Sherbrooke, Quebec, Canada.

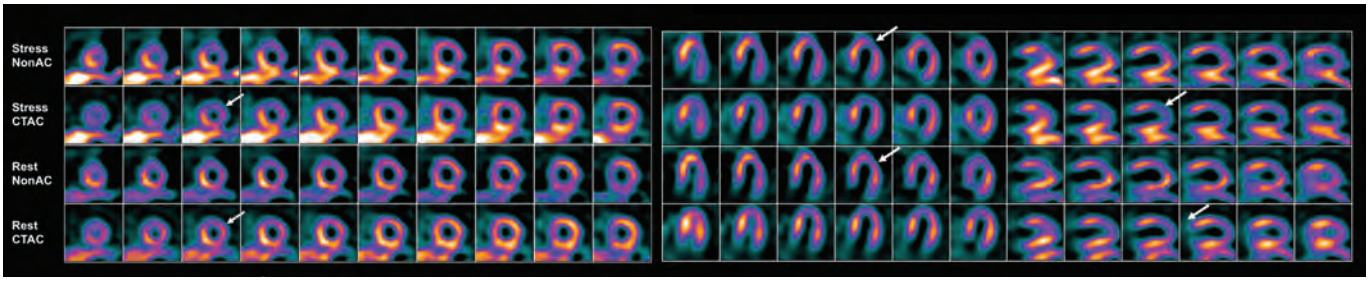


**Figure 21a:** Data courtesy of University of Sherbrooke, Sherbrooke, Quebec, Canada.

**Figure 21a:** A 60-year-old obese woman with a history of recurrent anginal pain underwent $^{99m}$Tc-MIBI IQ•SPECT with pharmacological stress and at rest. Study shows moderate perfusion defect in anterior wall, apex, and lateral wall, which appears reversible on the resting images. Small fixed defect in the anterior wall was interpreted as non-transmural infarction.

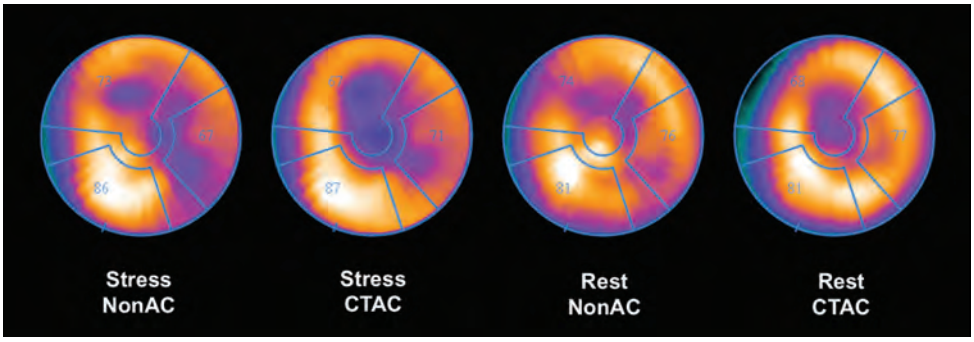


**Figure 21b:** Data courtesy of University of Sherbrooke, Sherbrooke, Quebec, Canada.

**Figure 21b:** Polar plots of the patient described above show the extent of reversible defect in anterior wall and a small area of fixed defect probably related to nontransmural infarction. Inferior wall, lateral wall, as well as septum, show normal perfusion. Percentage of ischemic myocardium was calculated as 25% of the LV by analysis of polar plot. Patient was referred for coronary angiography.

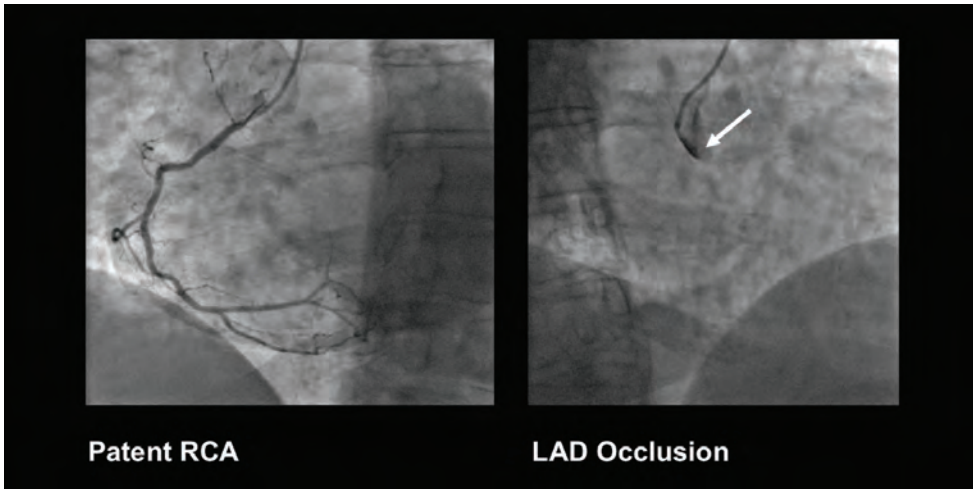


**Figure 21c:** Data courtesy of University of Sherbrooke, Sherbrooke, Quebec, Canada.

**Figure 21c:** Coronary angiography in this patient shows patent normal looking dominant RCA in this patient. LAD was completely occluded at the proximal level. Attempt to cannulate the occluded LAD was unsuccessful. In spite of the total LAD occlusion, the limited extent of LV ischemia was probably related to dominant RCA and good collateral circulation.

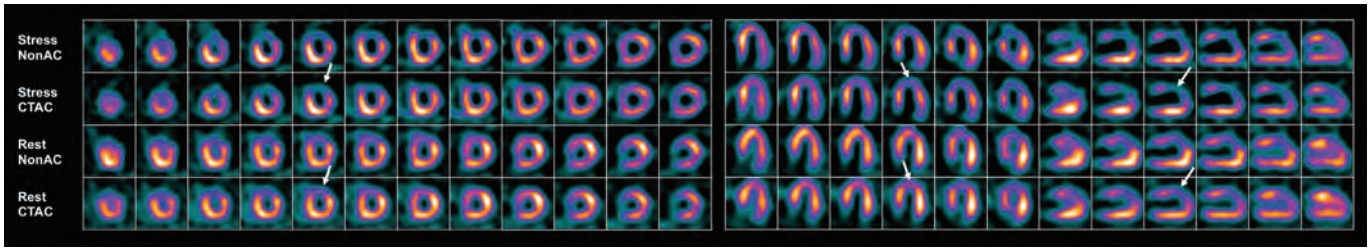


**Figure 22a:** Data courtesy of University of Sherbrooke, Sherbrooke, Quebec, Canada.

**Figure 22a:** A 79-year-old female with history of chest pain underwent $^{99m}$Tc-MIBI IQ•SPECT during treadmill stress and at rest. Study shows severe perfusion defect in anterior wall and apex with partial reversibility. Part of the anterior wall appears significantly thinned out with a fixed defect suggestive of nontransmural infarction.

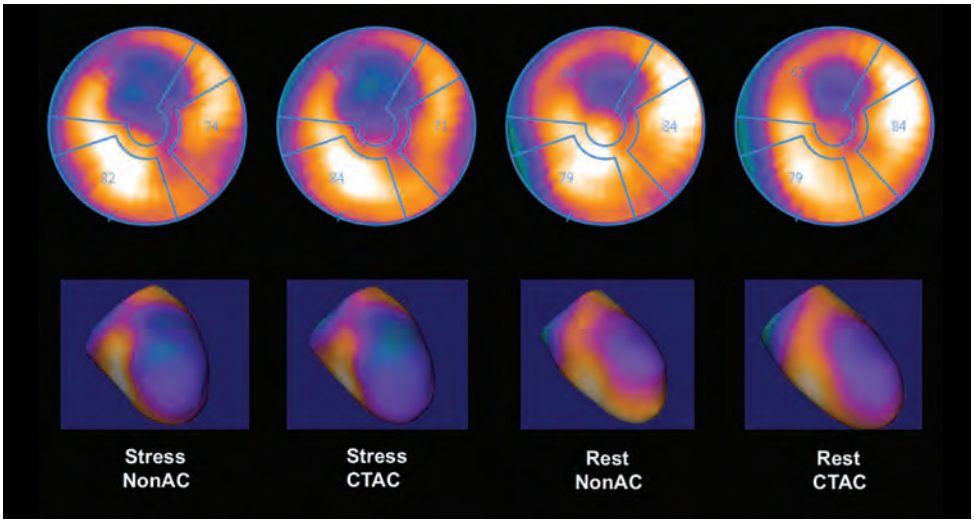


**Figure 22b:** Data courtesy of University of Sherbrooke, Sherbrooke, Quebec, Canada.

**Figure 22b:** Polar plots and volume-rendered images of the patient described above show large severe perfusion defect in the anterior wall and apex. The area of fixed defect in resting images suggests nontransmural infarction with significant reversible peri-infarct ischemia. Patient was referred for coronary angiography.

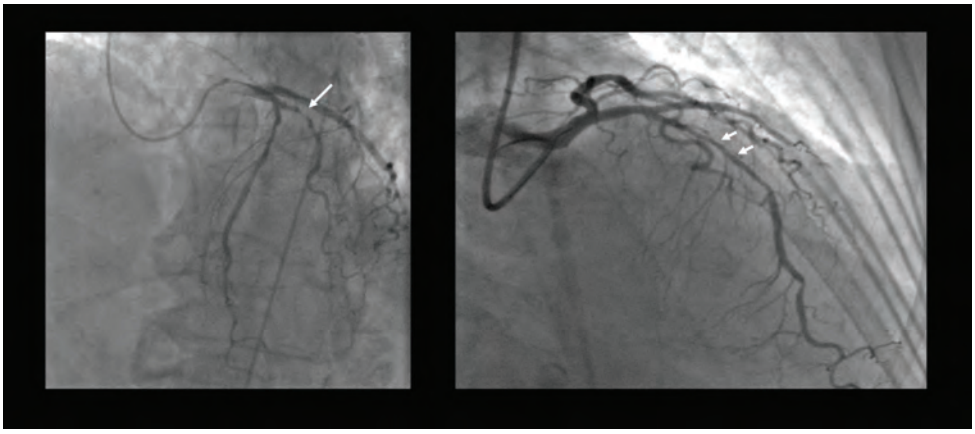

**Figure 22c:** Data courtesy of University of Sherbrooke, Sherbrooke, Quebec, Canada.

**Figure 22c:** Coronary angiography in the above patient revealed a sub-total occlusion of the first diagonal (D1) as well as diffuse moderate stenosis of mid-third of LAD (smaller arrows). There was also a mild proximal left circumflex stenosis. Patient underwent stenting of both D1 and LAD lesions.

Patterns of ischemia and reversibility are similar with both $^{99m}$Tc-MIBI and $^{201}$Thallium using IQ•SPECT. The following example of reversible ischemia visualized using $^{201}$Thallium and IQ•SPECT helps illustrate the point.

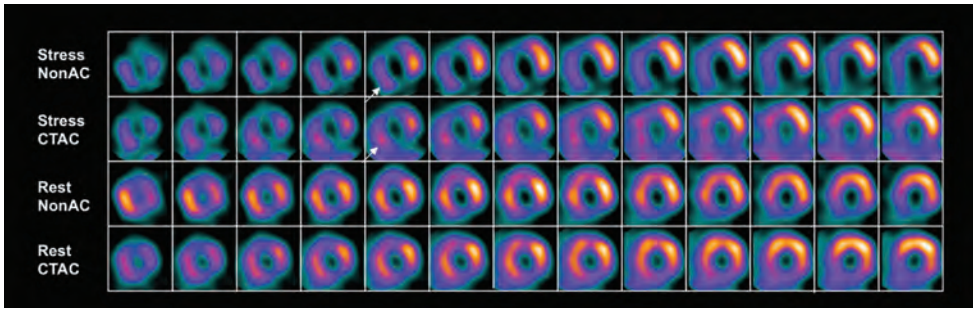


**Figure 23a:** Data courtesy of Chung Shan Medical University Hospital, Taichung City, Taiwan.

**Figure 23a:** A 58-year-old man with progressive dyspnoea on exertion underwent $^{201}$Thallium myocardial perfusion scanning at rest and with dipyridamole stress using IQ•SPECT. Short axis images show severe but reversible anterior and anteroseptal ischemia (LAD territory). Inferior and inferolateral walls also show reversible ischemia.

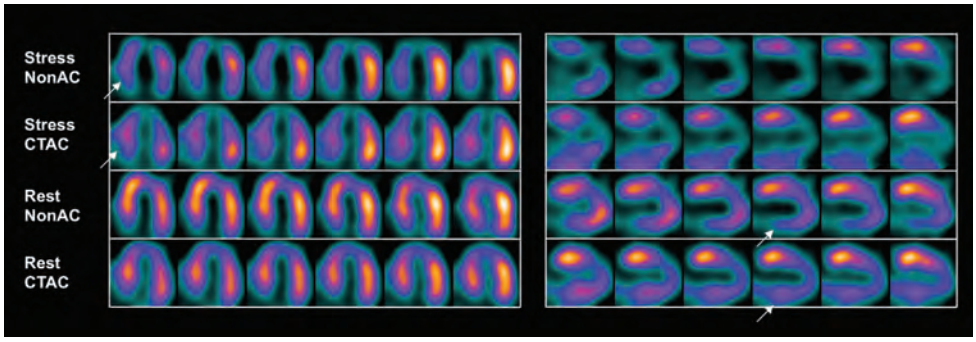


**Figure 23b:** Data courtesy of Chung Shan Medical University Hospital, Taichung City, Taiwan.

**Figure 23b:** Horizontal and vertical long axis views of the same patient show reversible ischemia in anterior, apical, anteroseptal, and inferior wall, suggestive of LAD and RCA lesion. Note the slight improvement in posterobasal uptake levels following CTAC, which helps define the true level of ischemia.

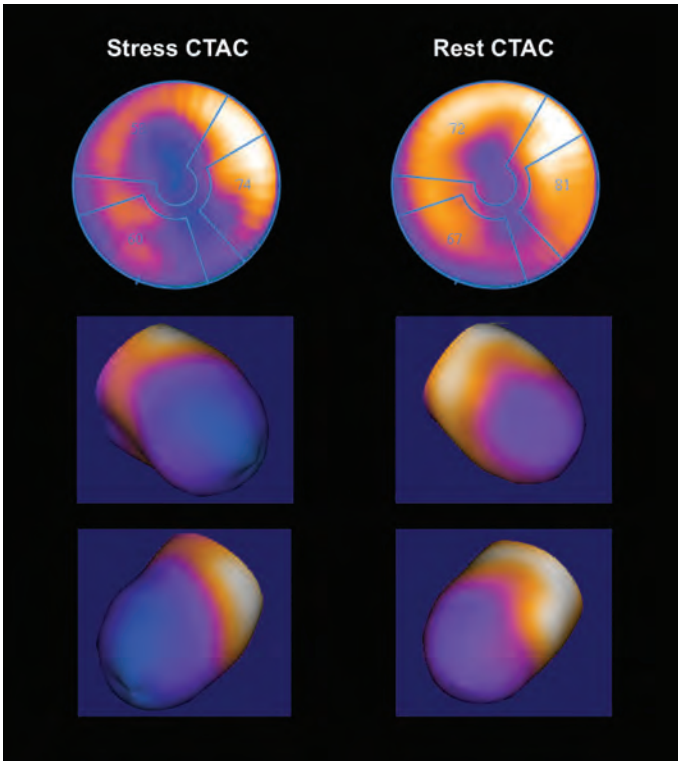


**Figure 23c:** Data courtesy of Chung Shan Medical University Hospital, Taichung City, Taiwan.

**Figure 23c:** Bulls-eye plots and LV volume renderings show severe ischemia in the apex, anterior, and anteroseptal walls, as well as the inferior wall. The lateral wall shows a normal uptake level. Note the post-stress LV dilatation, which reflects advanced disease. The patient was referred for coronary angiography.

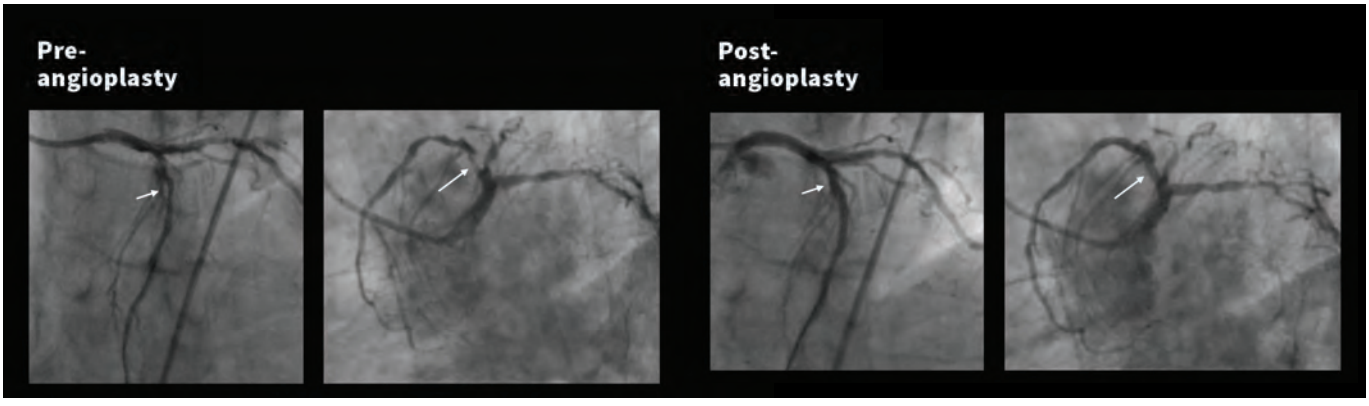


**Figure 23d:** Data courtesy of Chung Shan Medical University Hospital, Taichung City, Taiwan.

**Figure 23d:** Cardiac catheterization demonstrated severe (90%) proximal LAD stenosis, as well as moderate proximal RCA stenosis. A balloon angioplasty was performed at the same sitting, with improved coronary flow and fractional flow reserve following the procedure. The patient showed significant improvement in exercise tolerance following angioplasty.

# Conclusion

IQ•SPECT delivers ultrafast MPI with similar diagnostic confidence to LEHR, but with the advantage of high acquisition speed as well as the possibility of integrated diagnostic CT-based attenuation correction. Calcium scoring, in Symbia SPECT/CT systems equipped with that option, is an added advantage. As demonstrated in the series of clinical cases, normal as well as ischemic uptake patterns and defect sizes are comparable between LEHR and IQ•SPECT. Familiarity with normal patterns, attenuation effects, typical IQ•SPECT image characteristics, and cardiac shape differences helps improve clinical interpretation accuracy.

# Author

Partha Ghosh, MD
Dr. Ghosh is a clinical marketing advisor for Siemens Healthineers Molecular Imaging.

# Acknowledgements

1. Guillaume Bouchard MD, Consultant Physician, Department of Nuclear Medicine, Hopital de la Cite de la Sante de Laval, Canada
2. Sylvain Prevost MD, Director of Nuclear Medicine, University of Sherbrook, Quebec Canada
3. James Corbett MD, Director, Nuclear Cardiology, University of Michigan, Ann Arbor, MI USA
4. Ali Rahmy MD, Director, Nuclear Medicine, Atrium Medical Center, Heerlen, The Netherlands

# References

[1] Meden, J et al. (2011). Clinical comparison of four minute IQ•SPECT imaging with conventional parallel hole collimated SPECT/CT. SNM 2011, Abstract No. 1132.

[2] Corbett, J et al. (2011). Clinical validation of attenuation corrected cardiac imaging with IQ•SPECT SPECT/CT. SNM 2011, Abstract No. 1722.

[a] We also provide an alternate calibration protocol that does not offer the advantage of standardization, but can be used as a fall back in case the CSS is not available.

$^{99m}$Tc antigranulocyte antibody referenced herein is not currently recognized by the US FDA as being safe and effective, and Siemens does not make any claims regarding its use.

$^{90}$Y-DOTATOC is not commercially available in some countries, including the US. $^{90}$Y-DOTATOC is not currently recognized by the US FDA as being safe and effective, and Siemens does not make any claims regarding its use. Due to regulatory reasons, its future availability cannot be guaranteed. Please contact your local Siemens organization for further details.

**Siemens Healthineers Headquarters**
Siemens Healthcare GmbH
Henkestr. 127
91052 Erlangen, Germany
Phone: +49 9131 84 0
siemens.com/healthineers

**Published by**
Siemens Medical Solutions USA, Inc.
Molecular Imaging
2501 North Barrington Road
Hoffman Estates, IL 60192
USA
Phone: +1 847 304-7700
siemens.com/mi

*Order No. A91MI-10476-T1-7600 • Printed in USA • All rights reserved • MI-3698.TM.JV.TW.1500 • © Siemens Healthcare GmbH, 04.2018*